NEUROPROSTHETIC DEVICE FAILURE ANALYSIS: IMPACT OF SHEAR STRESS AND BLOOD-BRAIN BARRIER DISRUPTION

by

FATEMEH KHODADADEI

DISSERTATION

Submitted to the Graduate School

of Wayne State University,

Detroit, Michigan

in partial fulfillment of the requirements

for the degree of

DOCTOR OF PHILOSOPHY

2022

MAJOR: MATERIALS SCIENCE AND ENGINEERING

Approved By:

_____

Advisor Date

_____

_____

_____

_____

ACKNOWLEDGEMENTS

First and foremost, I would like to express my heart-felt gratitude to my advisor, Professor Carolyn Harris. Professor Carolyn is someone you will instantly love and never forget once you meet her. I would like to thank her for her invaluable supervision and continuous support that has given me the freedom to pursue various projects during my PhD study. Her excitement for new research always fascinated me and I have been greatly influenced by her to be a mature researcher. I was lucky to be in her lab and would not be able to achieve what I have done without her guidance.

I am also very grateful to Professor Allen Liu for his support, scientific advice, and extremely knowledgeable suggestions during my PhD study. His insightful feedback guided me to sharpen my thinking and brought my work to a higher level.

I would also like to thank my great committee members, Professor Howard Matthew, and Professor Haipeng Liu, for their invaluable guidance on my prospectus. They provided me with the suggestions that I needed to choose the right direction and successfully complete my PhD study.

TABLE OF CONTENTS

LIST OF FIGURES

Chapter 1. Introduction

Like a well-guarded fortress, the brain defends itself from invaders. A common invader is bacteria, which the brain defends against by signaling, surrounding, and consuming. We recover and move on. However, if the invader is an implanted device, a neuroprosthetic, the brain attacks but cannot consume its target. No matter the device's purpose, this inflammatory foreign body response (FBR) continues until the device is barricaded from normal brain tissue, rendering it totally ineffective. This can occur anywhere from days to months after implantation. Still, neuroprosthetics have become a $14 billion global market for the 1 billion people suffering from long-term neurologic deficits. Patients with drug-resistant Parkinson's disease, ALS, paralysis, cervical spine injury, and hydrocephalus are commonly treated with neuroprosthetics to stimulate, record, or divert fluid in the brain [1]. As stimulators, neuroprosthetics drastically minimize tremors and improve rigidity. As biosensors, neuroprosthetics inform scientists and clinicians about memory, plasticity, and behavior. And with neurological disorders like hydrocephalus, neuroprosthetics designed to reduce intracranial pressure are the only currently viable treatment. Patients with hydrocephalus show that the unacceptably high 98% failure rate of these neuroprosthetics is due to the FBR: inflammatory glial cells attach, activate, proliferate, and surround the device until total failure occurs [2], [3].

1.1. Hydrocephalus

Hydrocephalus is a neurological disorder defined by an abnormal buildup of cerebrospinal fluid (CSF) in the ventricles of the brain. This devastating disease has no known cure and is treated using a chronically implanted shunt system, which is critical in reducing intracranial pressure via diverting excess CSF from the brain to other parts of the body. Unfortunately, these important medical devices are plagued with a high rate of failure of up to 40% within the first two years post-implantation and up to 98% within 10 years due to mechanical blockage of ventricular catheter inlet pores, imposing a significant burden on patients, their families and society. Understanding the root causes of shunt failure to design improved implantable devices, will indeed reduce costly shunt replacement surgeries and therefore an overall reduction in morbidity/mortality. Although hydrocephalus may be acquired in life due to incidents such as head trauma or tumor development, approximately one in every 1000 newborns is diagnosed with congenital hydrocephalus. The annual cost of hospital care for treating pediatric hydrocephalus patients is estimated to exceed $2 billion in the United States. A large portion of shunt failures can be attributed to occlusions at the ventricular catheter due to inflammatory reaction, blood clots, or choroid plexus tissue ingrowth. Although there have been attempts to use in situ clearing methods using laser, ultrasound, electrocautery or microactuators to remove catheter obstructions, these surgical interventions did not attain wide acceptance due to their invasiveness.

Hydrocephalus happens when cerebrospinal fluid (CSF) does not drain out of the ventricles due to an imbalance between the rates of CSF production and absorption. CSF

is the saltwater that surrounds and cushions the brain and spinal cord. Shunts are placed to treat hydrocephalus by draining the extra fluid and help prevent pressure from getting too high in the brain. A shunt is a thin plastic tube with a distal and proximal polydimethylsiloxane (PDMS, silicone) catheter.

Despite the controllable modifications of shunt design, the shunt systems have undergone limited technological advancements. The current design used for hydrocephalus treatment is plagued by high failure rates, mostly due to obstruction with inflammatory cell activation and attachment on the shunt surface (Figure 1.1). Recent data collected in our lab validate other reports indicating that the shear stress produced on the shunt surface are one of the primary factors involved in astrocyte cell attachment and aggregation on shunts [4], [5]. Therefore, there is a clear need to investigate these relationships further since we can manipulate these shear forces through simple modifications of shunt design to reduce astrocyte cell activation and attachment to reduce shunt device failure rates for the next-generation medical devices.

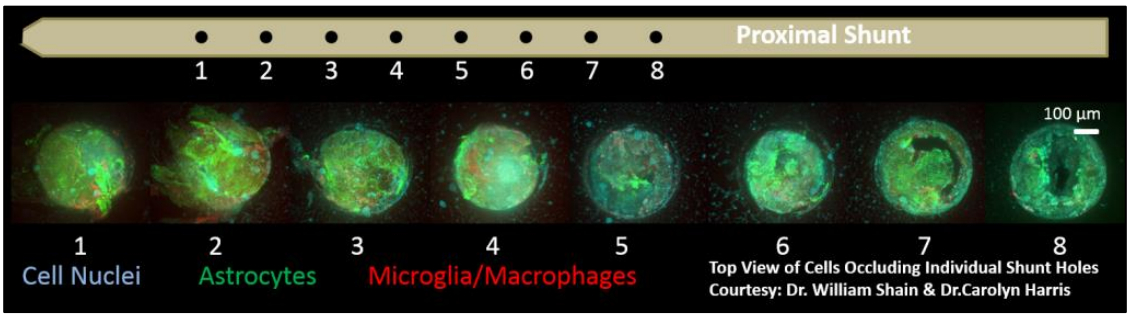

Figure 1.1. Astrocytes/macrophages are the dominant cell types bound directly to shunt surfaces.

To improve hydrocephalus shunts the shear forces can be manipulated to reduce device failure. And unlike shear stress in other areas of the brain caused by blood flow, for instance, we can control shear stress on the shunt surface by specifically manipulating the shunt geometry [6].

1.2. Inflammatory foreign body response to neuroprosthetics

Penetrating cortical medical devices are a critical component to directly monitor and reduce disease symptoms for a dramatic improvement in the patient quality of life. In the past decade, there has been a rise in the identification of chronic neurologic disease, and an increase in demand for new treatment paradigms besides pharmacological interventions that are inconvenient or completely ineffective. Neuroprosthetics are novel treatments designed to provide safe levels of therapeutic neuronal stimulation, record large ensembles of neurons for cognitive control, and can normalize the deadly increase in intracranial pressure inside the adult or developing brain. However, while the implants have demonstrated enormous potential, large variability of implant performance and poor longitudinal reliability has been a major challenge limiting the adoption of this technology. This variability and unreliability are understood to be the result of complex multimodal failure mechanisms. The common concept of initial failure mechanisms is biomaterial-based damage or the vasculature or blood-brain barrier (BBB) disruption upon implantation in the cortex that elicits a foreign body response (FBR), resulting in chronic inflammation that leads to poor implant performance.

1.2.1. Rapid inflammatory response in early-stage implantation

Implantation of foreign materials within the brain initiates a series of reactions, collectively called the foreign body reaction (FBR), which intends to eliminate or separate the implanted foreign material from the host immune system. Upon implantation of large medical devices such as neuroprosthetics, where elimination is not possible, the FBR continues until the device is barricaded from healthy brain tissue. The initial phase of the FBR is blood-device interactions, which occurs immediately upon implantation caused by vasculature or blood-brain barrier (BBB) disruption (Figure 1.2). This results in the nonspecific adsorption of blood proteins to the device surface through a thermodynamically driven process to reduce surface energy. Other than BBB disruption and influx of serum proteins, the immune system is also activated by signals of host cell injury and extracellular matrix (ECM) breakdown proteins such as fibrinogen and fibronectin adhesion to the device surface [7], [8]. Microglia, the resident immune cells of the central nervous system (CNS), and blood-derived macrophages recognize the protein signals through receptor-mediated pathways such as toll like receptors (TLRs). Ligand binding to TLRs leads to activation of microglia/macrophages and the secretion of pro-inflammatory cytokines such as TNF-α, IL-1α, and IL-1ß [9]–[11]. These very potent signaling molecules are rapidly upregulated in the injured CNS, and are observed right at the device-tissue interface corresponding to the location of activated microglia/macrophages and exaggerated astrocytes [10], [12], [13]. The effect of TNF-α and IL-1β is strongest on astrocyte activation and proliferation, the key member of the CNS immune response. Reactive astrocytes form a physical barrier, known as glial scar, where

newly formed and hypertrophic astrocytes overlap and play a beneficial role to inhibit injury from extending to nearby healthy tissue. However, in relation to its effect on implants, the glial scar is considered undesirable because, regardless of the device type, elicits failure [14], [15]. Collectively, the dominant role of cytokines in orchestrating the dynamic crosstalk among cells and mediating device failure is evident.

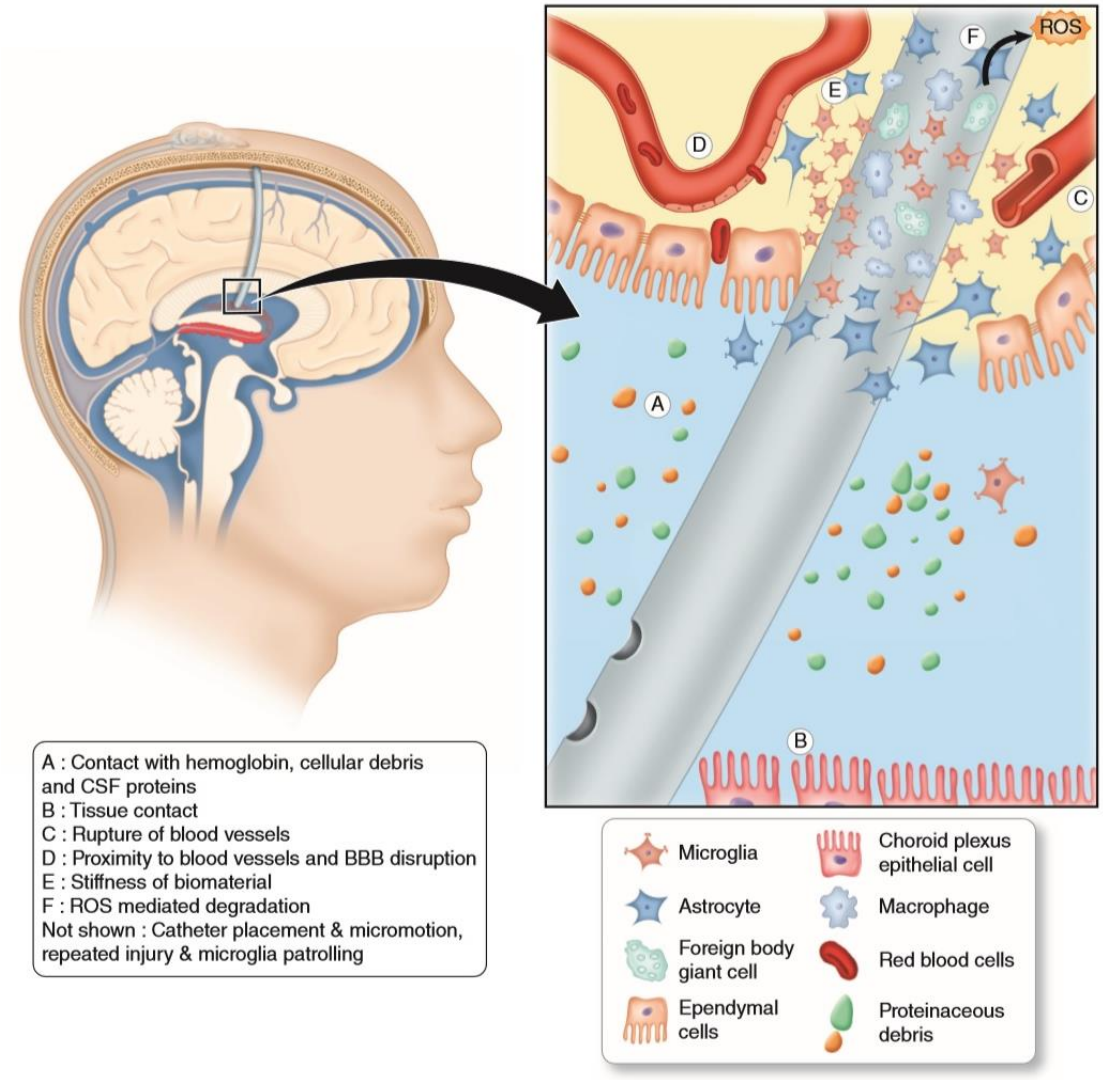

Figure 1.2. Blood-brain barrier disruption upon implantation elicits a foreign body response [16].

Due to high vascularization of the central nervous system tissue, hydrocephalus shunt implantation inevitably causes the damage of localized vasculature that results in protein adsorption on the shunt surface. Thus, activating inflammatory cells to release inflammatory cytokines that promote blood-brain barrier (BBB) disruption and persistent neuro-inflammatory foreign body response (FBR).

1.2.2. Cytokines

Cytokines are key biomolecules acting as mediators and modulators of the complex immune system. They are low molecular weight and soluble proteins secreted by immune cells to adjust cell-to-cell communication. The complex roles of cytokines in providing an immunity balance have attracted interest in its quantification and application for disease treatment and drug advancement. For instance, the dynamic transition of the immune status from excessive production of pro-inflammatory cytokines, for example TNF-α are counteracted by certain anti-inflammatory cytokines, including IL-10, TGF-β, and IL-4, which aim to restore immunological equilibrium within a short period of time

Cytokines and inflammatory stimuli have powerful impacts on astrocyte gene expression and physiology that can significantly affect synaptic and neuronal functions. The different astrocyte signaling abilities mediate the crosstalk between immune systems [17].

1.2.3. Astrocytes

Astrocytes are glial cells of neural progenitor origin that contiguously tile the central nervous system (CNS) where they constitute one of the most abundant cell populations and provide multiple activities essential for CNS functions in health and disease. Astrocytes interact with neurons and their synapses, oligodendrocyte progenitor

cells, microglia, various perivascular cells, meningeal fibroblasts, and circulating immune cells. In healthy CNS tissue, astrocytes maintain homeostasis of extracellular fluids, ions, and transmitters, provide glucose metabolites as energy substrates to neurons, modulate local blood flow, help to regulate drainage of interstitial fluid, play essential roles in synapse development and plasticity, and exhibit dynamic activities that are crucial for neurological functions. Other than having an important impact on healthy tissue, astrocyte roles are significant in all CNS diseases. Astrocyte reactivity is a critical factor of CNS innate immunity that can lead to a diverse set of potential changes in astrocyte morphology, molecular expression, and functions that can influence outcomes in all types of CNS disorders including traumatic injury, autoimmune inflammation, microbial infections, tumor formation, exposure to environmental toxins, peripheral metabolic disorders, and neurodegenerative diseases. Astrocytes are increasingly implicated in influencing disorder outcome. As information grows, astrocytes will increasingly become targets for therapeutic interventions. Reactive astrocyte subtypes derive from their function. Two fundamentally different subtypes are astrocytes that are anti-inflammatory, proliferative and migrate to form new borders around tissue damage with inflammation, and astrocytes that are not proliferative but hypertrophic and pro-inflammatory.

1.2.3.1. Proliferative, border-forming, reactive astrocytes

These surround damaged tissue that contains leukocyte infiltration, stromal-cell proliferation, and fibrosis after trauma, ischemia, infection, autoimmune inflammation, toxin accumulation, blood brain barrier (BBB) leakage, or neurodegenerative disease.

These new astrocyte borders separate and isolate damaged, inflamed, and fibrotic tissue from adjacent viable neural tissue in a manner analogous to the astrocyte limitans borders that isolate non-neural from neural tissue along the meninges in healthy CNS. Border-forming reactive astrocytes interact with non-neural stromal and immune cells which they attract, instruct, and corral. Border-forming astrocytes are essential for reforming the BBB around lesions, as well as for protecting and preserving adjacent functional neural tissue, such that loss or attenuation of these cells leads to increased spread of inflammation and serum proteins, increased loss of neural tissue, and decreased functional recovery in rodents. New astrocyte borders and reorganized tissue architecture are essentially permanent. Newly proliferated astrocytes can derive from different progenitor sources, including proliferation of local astrocytes and periventricular neural progenitors. At present, it appears that proliferation of reactive astrocytes is associated primarily with border formation, and that most border-forming astrocytes around CNS lesions are newly proliferated. Because astrocytes divide rarely in healthy tissue, proliferation is an important means of discriminating between different subtypes of reactive astrocytes; those that proliferate and those that do not. In constructing a complex scar-like coating that reduces volume diffusion, reactive astrocytes have a function comparable to reactive fibroblasts.

1.2.3.2. Non-proliferative hypertrophic reactive Astrocytes

These maintain their locations and fundamental features of cell structure, cellular interactions, and functions in neural tissue that is not overtly damaged and retains its tissue architecture, but nonetheless responds to injury or disease. Depending on the nature and

severity of the insult, non-proliferative reactive astrocytes exhibit variable changes in molecular expression and variable degrees of cellular hypertrophy. Notably, the discrete, nonoverlapping cellular domains exhibited by astrocytes in healthy grey matter are preserved such that hypertrophy occurs primarily within these individual cellular domains. Thus, non-proliferative reactive astrocytes are likely to continue to functionally interact with the same cellular elements that they interact with in healthy tissue, including for example, neurons, synapses, and blood vessels. Non-proliferative astrocyte reactivity can resolve over time if acute triggers recede. Astrocyte reactivity can become chronic if triggers persist.

1.2.3.3. Reactive astrocytes and CNS innate immunity

Reactive astrocytes are integral and essential components of multicellular CNS innate immunity. Astrocytes respond to activators of innate immune responses, including all forms of microbial pathogens, environmental toxins, and diverse forms of tissue damage. Astrocytes exchange molecular signals and interact directly with other innate immune cells such as microglia, various perivascular cells, and blood-borne leukocytes. Astrocytes can both elaborate and respond to a wide variety of cytokines, chemokines, growth factors, and other molecules that mediate intercellular communication during innate immune responses. Reactive astrocytes can attract, instruct, and corral inflammatory and immune cells to form adventitial cuffs that harbor foci of activated immune cells in an extracellular matrix. Astrocyte processes form tight junctions which restrict or corral immune cells within the cuffs space when blood-borne leukocytes cross the endothelial

BBB. Astrocyte borders around such cuffs may serve to attract and then restrict the spread of bloodborne immune and inflammatory cells. At sites of CNS damage astrocyte scar borders are formed by newly proliferated anti-inflammatory astrocytes that construct a functional barrier to inhibit diffusion of inflammatory molecules and cytotoxic factors. Thus, to resolve inflammation over time scar-forming astrocytes recruit and restrict or confine inflammatory cell migration such as leukocytes and microbial pathogens through signal transducer and activator of transcription 3 (STAT3) signaling pathway [18].

Astrocytes are extremely sensitive to infection-associated toll-like receptors (TLRs) and cytokines, which can drive astrocyte phenotype towards highly pro-inflammatory and cytotoxic phenotypes. Such responses are initiated by local microbial infections and are damaging. Thus, astrocytes exposed to TLRs could promote the recruiting of cytotoxic leukocytes (neutrophils, eosinophils, and macrophages) to CNS insults.

Why study reactive astrocytes:

1. Reactive astrocytes are increasingly implicated in influencing disorder outcome and are increasingly becoming targets for therapeutic interventions.
2. Reactive astrocytes attract, instruct, and corral inflammatory and immune cells to form adventitial cuffs that harbor activated immune cells in an extracellular matrix, which engulf the implanted device leading to failure.
3. Reactive astrocytes are highly mechanosensitive cells that certainly sense micromotion induced shear forces at the brain-device interface.

1.2.4. Microglia/Macrophages

Chief among CNS glial cells are microglia/macrophages as well as astrocytes. Microglia, the brain-resident macrophages, are regarded as the innate immune cell of the CNS, continuously monitoring their surroundings to sense and resolve any disturbance. Given their well-established role as immediate responders to injury and infection it is not surprising that dysregulation of microglial activation and induced inflammation is observed in all brain neuroinflammation disorders. Blood-borne macrophages are also essential component of the disease related microenvironment in the brain and are regarded as critical mediators of progression in neuroinflammation disease.

Both microglia/macrophages and astrocytes have pro- and anti-inflammatory functions dependent on the mode of injury. Recently, resident microglia and infiltrating macrophages have been implicated in driving astrocyte reactivity. Coordinated interactions of these cells are essential for the control of the inflammatory response. Based on literature, shear stress has a direct stimulation impact on astrocytes, but less impact on microglia/macrophages [14], [19], therefore the effect of shear stress on astrocytes is investigated. Astrocytes directly sense mechanical stress and are activated to rapidly increase cytokine secretion that have been associated in the initiation of the glial scar formation.

Chapter 2. Motivation for research

Shear stress acting on medical devices implanted in the brain is shown to significantly accelerate device failure rate in unfortunately millions of patients across the US with chronically indwelling neuroprosthetics. These motion-induced shear forces at the device–brain interface exacerbates a complex and more importantly a continuous cascade of foreign body reactions. Continuous motion of the brain with respect to the device induces an ongoing damage to the surrounding tissue, which in turn will severely compromise the device performance. Shear forces inside the brain are cardiac rhythm, fluctuation in respiratory pressure, interstitial fluid flux, and cerebrospinal fluid (CSF) flow. Fortunately, in the latter case, the shear forces can be manipulated to reduce device failure. This is the case for hydrocephalus shunts, devices used to chronically divert excess CSF away from the brain to reduce intracranial pressures. Unfortunately, the shunt systems have undergone limited technological advancements. The current design used for hydrocephalus treatment is plagued by 98% failure rates. Recent data collected in our lab corroborate other reports indicating that motion-related shear forces are one of the primary factors involved in significantly accelerated inflammatory cell (astrocyte) activation and attachment on the shunt surface. And unlike shear forces in other areas of the brain caused by blood flow, we can control shear forces on the shunt surface by specifically manipulating the shunt geometry. Therefore, there is a clear need to investigate these relationships further since we can manipulate these shear forces through simple modifications of shunt design to reduce astrocyte cell activation and attachment to reduce shunt device failure rates for the next-generation medical devices.

One way, astrocyte cells rapidly communicate and manipulate their activation/attachment is via cytokine secretion, specifying them as the most important measurable outcome for neuroinflammatory cascades. Shear stress mechano-sensors of astrocyte cells are proteins located throughout the cell membrane and cytoskeleton. Activation of these naturally derived flow-sensors upon shear stress leads to alteration of cellular signaling and cytokine secretions. Cytokine secretions from cells create spatially and temporally varying concentration profiles in the extracellular environment, which leads to a wide range of cellular responses. Thus, we hypothesize that along the shunt/CSF interface, shear stress activated astrocyte cells secret cytokines which in turn cause activation of other astrocyte cells and eventually exaggerated cell proliferation and aggregation and ultimately shunt device failure.

In a recent world-renowned study, Barres and his colleagues identified two significantly different reactive astrocyte phenotypes, which they called A1 and A2. A breakthrough to understanding cellular response mechanism to device implantation is to discover whether there are A1 or A2 astrocytes on the shunt surface. Hence, enabling the precise search for cues initiating and attenuating the reactive cellular response to implanted devices.

In this study, we develop a better understanding of shear forces at the medical device interface. We study inflammatory cell activation and cytokine secretion dependent on shear forces to identify root causes for shunt failure. We present a real-time quantitative analysis and direct spatial-temporal mapping of secreted cytokines upon shear stress at the

single cell level. Furthermore, in this study for the first time we explore astrocyte phenotype expression on implanted devices.

2.1. Single cell real-time cytokine secretion under shear stress

To obtain a high enough sensitivity and resolution for single cell studies, restrictive experimental conditions such as low cytokine density need to be imposed. The key to a successful and feasible outcome is attributed to synergistically employing microfluidic devices for noninvasive mechanical stimulation of single cells and total internal reflection fluorescence microscope (TIR-FM) for single cell real-time cytokine detection. Combining microfluidic devices with TIR-FM, can provide the correlations between mechanical stimulation and fluorescence signals. Here, the amount of cytokine secreted from a single cell is correlated to the shear stress applied on the single astrocyte cell. Hence, we quantify and analyze secreted cytokines under shear stress, which are known to induce shunt device failure. Thus, the unique microfluidic/TIR-FM biosensor will serve as a new and powerful tool to reduce device failure rates. Furthermore, microfluidic devices are polydimethylsiloxane (PDMS) based materials replicating CSF shunts. To mimic the shunt surface, PDMS microfluidic device are coated with fibronectin. Then, ELISpot analysis is to confirm increase in cytokine secretion from astrocyte cells under shear stress.

2.1.1. The relationship between device failure and shear stress

First time comprehensive picture of single cell real-time cytokine secretion upon shear stress for applications in which a misunderstanding of device failure has plagued device design for decades.

The pro-inflammatory cytokine pathway is the best and most important measurable outcome for neuroinflammatory cascades. Inflammatory cells at the brain-device interface communicate via pro-inflammatory cytokines to recruit other inflammatory cells to the interface. Pro-inflammatory cytokine stimulation is a gateway for other gene products to be over- or under-expressed in the cascade resulting in device failure. Therefore, it is a starting point for mechanistic and thorough investigation of neuroinflammation and device failure.

Modifications have been made over the last decade to inhibit inflammatory cell activation and attachment on medical devices implanted in the brain. However, all implanted devices continue to chronically fail. In this study we show that the opportunistic neuroinflammatory response is significantly accelerated under motion-related shear forces inside the brain. Therefore, investigating these relationships further and manipulate these shear forces through simple modifications of shunt design open new avenues to reduce shunt device failure rates for the next-generation medical devices. Thus, the unique microfluidic/TIR-FM biosensor will serve as a new and powerful tool for single cell real-time cytokine secretion dynamics under shear stress.

By themselves, standard cell culture techniques and animal models cannot be used to understand cellular mechanisms and communication because of the known heterogenous

response (ensemble averaging) of astrocytes. Single cell methods can provide unprecedented, detailed information about dynamic behavior as well as transient and rare or unlikely cellular states which complement bulk assays. Similarly, complex spatiotemporal distributions and properties of ensembles of cytokines for an individual cell can be revealed.

Different patterns of single cell real-time cytokine secretion upon shear stress are: one directional/multidirectional, autocrine/paracrine, continuous/concentrated burst, as a function of time. Cells release some cytokines in one direction to impart specific cell-to-cell communication and others multidirectional to promote inflammation and to establish chemokine gradients. Therefore, the novel microfluidic/TIR-FM biosensor allows for a broader and remarkable use for direct quantitative study of cell-to-cell communication.

literature show that protein concentrations around an implanted device dictate cell attachment, spreading, and subsequent cytokine secretion from cells [20], [21]. The type of adsorbed protein on a device surface manipulates the degree of cell cytokine release. Vascular damage initiates the exposure of neuroprosthetic devices to an influx of pro-inflammatory ECM proteins [22]. The innovative microfluidic/TIR-FM biosensor allows to coat the PDMS microfluidic device with different ECM proteins to observe different cytokine secretion from cells under shear stress. The clear advantage of our findings over existing data is analysis at the single-cell level as a function of time for clear understanding of mechanism of protein-cell inflammatory signaling under shear stress.

2.2. A1/A2 reactive astrocyte phenotype expression on the device surface

We collect failed shunts from patients to observe whether the cells on the shunt surface are expressing A1 or A2 astrocyte phenotype. A powerful marker for A1 astrocytes is the complement component C3, specifically upregulated in A1 reactive astrocytes (and not in resting or A2 reactive astrocytes). This marker provides an invaluable way to distinguish between different activation states of reactive astrocytes. EMP1 is an A2-specific gene. We use RNAscope fluorescent in situ hybridization and quantitative PCR analysis to determine the A1 or A2 reactive astrocyte phenotype expression on failed shunt. ELISA analysis confirms the pro- and anti-inflammatory cytokine concentration profiles in the CSF associated with astrocyte activation. This aim will shed light on which astrocyte phenotype is expressed on the shunt surface.

2.2.1. The relationship between device failure and astrocyte activation

First-time revealing of astrocyte phenotype expression on implanted medical devices for simultaneous manipulation of shunt design and targeted therapies for significant reduction in device failure.

In a recent world-renowned study, Barres and his colleagues observed that in human neuroinflammatory diseases resting astrocytes transform into A1 and A2 reactive astrocytes, which are primed to produce large volumes of pro-inflammatory and anti-inflammatory cytokines. In every neuroinflammation case, they observed large numbers of A1reactive astrocytes preferentially clustering where the disease was most active. Likewise, all implanted medical devices in the brain elicit the same neuroinflammatory

response, which leads to loss of device function. However, the astrocyte phenotype expression on the device remains mysterious. For the first time in this study, we observe if the active site on the shunt surface is also expressing A1 or A2 reactive astrocytes. A precise understanding of cellular response mechanism to device implantation presents: (1) a precise selection of cell phenotype for shear stress experiments for a precise interpretation of failure in chronically indwelling neuroprosthetics, (2) a therapeutic window for more targeted therapies. A1 and A2 astrocyte activation and attachment on the implant could be prevented by delivery of neutralizing antibodies to TNFα, IL-1β, and IL-1α (cytokines inducing A1 and A2 reactive astrocytes). FDA-approved drugs targeting TNFα, IL-1β, and IL-1α already exist and are in use for other medical conditions. Therefore, to prevent device failure, alongside manipulating shunt geometry, drug therapy is used for inhibition of cytokines and therefore inhibition of cell aggregation.

Chapter 3. Neuroprosthetic device failure dependent on shear stress?

The material in chapter 3 has been reproduced from the published article “A high-resolution real-time quantification of astrocyte cytokine secretion under shear stress for investigating hydrocephalus shunt failure” with permission of the publisher [23].

3.1. Introduction to the study

Neuroprosthetic devices implanted in the brain are significantly affected by shear forces that accelerate the rate to device failure in patients. For patients with hydrocephalus and high intracranial pressure, cerebrospinal fluid (CSF) shunts are nearly the only treatment paradigm of long-term surgical management of hydrocephalus, yet shunts are plagued by 98% failure rates. Recent evidence has indicated this to be mostly due to obstruction of the shunt system with adherent inflammatory cells (involving astrocytes, macrophages, and microglia). Since we know that astrocyte adhesion appears to be susceptible to changes in flow, we hypothesized that shear stress on the shunt surface significantly accelerates astrocyte activation. One way astrocyte cells rapidly communicate and manipulate their activation/attachment is via shear stress-dependent cytokine secretion. Quantitative analysis and direct spatial-temporal mapping of secreted cytokines at the single-cell level under physiological shear stress provides valuable information to identify root causes for shunt failure. Here, we acquire these data using microfluidic enabled patterning for noninvasive mechanical stimulation of single cells and a highly sensitive/selective total internal reflection fluorescence microscope (TIR-FM) for live single cell cytokine detection. Real-time secretion imaging allowed successful detection of

a significant increase in fluorescence intensity for IL-6 cytokine secretion under high shear stress of more than 0.5 dyne/cm^2, indicating that shear stress activates astrocytes. The TIR-FM platform also helped in elucidating the real-time cytokine secretion on different substrates with and without fibronectin (FN), for an appropriate representation of the in vivo occurrence of inflammatory response on CSF shunts. Ultimately, our microfluidic/TIR-FM biosensor will serve as a powerful tool to refine our misunderstanding of device failure that has plagued device design for decades.

3.2. Literature review

Persistent motion-related shear forces of medical devices implanted in the brain triggers a rather complex cascade of foreign body reactions (FBR) when compared to the initial iatrogenic trauma, culminating in high device failure rates [24]–[26]. There is a striking difference with initial mechanical-insertion-induced acute injury and chronic tissue inflammation from indwelling probes. The primary mechanism is exacerbated glial response around anchored devices caused by micromotion and/or shear stress [14], [19], [27]–[31]. Brain motion-related shear forces arise from physiological sources such as cardiac rhythm, fluctuation in respiratory pressure, maneuvering interstitial fluid, and in the case of shunt systems used to treat hydrocephalus, cerebrospinal fluid (CSF) flow. In standard shunts, most of the CSF volume flows through the proximal holes of the shunt's ventricular catheter, i.e., holes located furthest from the tip of the shunt with less resistance to flow. This fact increases the shear stress at the proximal segment and is one of the most important factors of high shunt device failure rates [4], [32]. Recent data collected in our

lab corroborate other reports suggesting that inflammatory astrocyte attachment to shunts is correlated to a change in flow rate through the shunt holes and indirectly, the shear rate through these holes [33]–[36]. Fortunately, unlike shear stress in other areas of the brain, we can control shear stress on the shunt surface by specifically manipulating the shunt geometry. Therefore, there is a clear need to investigate these relationships further since we can manipulate these shear forces through simple modifications of shunt design to reduce astrocyte cell attachment and shunt device failure rates.

Astrocytes directly sense mechanical stress through activation of cell membrane flow-sensors, and translate it into cellular signaling, such as rapid increase in cytokine secretion. Cytokine secretion creates spatially and temporally varying concentration profiles in the extracellular environment, which leads to a wide range of cellular responses. Along the shunt/CSF interface, shear stress activated astrocytes secret cytokines which in turn cause activation and proliferation of other astrocytes and eventually glial scar formation on the device surface.

Several groups have reported analysis of cytokine secretion from cells [37]. These methods cannot currently offer either a time interval of shorter than a few hours nor simultaneous real-time monitoring of a second intracellular variable (e.g., cell viability) over time. A methodology with a label-free technique based upon nano-plasmonic imaging has been developed [38], [39]. Plasmonic nano-biosensors rely on the interaction of electromagnetic radiation on a noble metal in contact with a surrounding dielectric medium. When the collective motion of the free electrons in a metal resonates with an incident light wavelength, surface-confined electromagnetic modes referred to as surface

plasmons are created. Surface plasmons possess an evanescent field at the boundaries between the metal and the dielectric region. The adsorption of biomolecules in the vicinity of the metal–dielectric interface results in the alternation of the resonant condition of surface plasmons, which enables real-time quantitative analysis of biomolecular density [40]. However, since the plasmonic signal is proportional to the molecular weight of the binding molecule and cytokines are small proteins, a more sensitive and specific approach is required. Conjugation of an analyte to other proteins could amplify an image signal as observed in sandwich immunoassay, where the analyte is sandwiched between capture and secondary antibodies.

To better understand inflammatory cell activation and cytokine secretion dependent on shear stress, a real-time quantitative analysis and direct spatial-temporal mapping of secreted cytokines upon shear stress at the single cell level was developed. To obtain a high enough sensitivity and resolution for single cell studies, restrictive experimental conditions such as low cytokine density need to be imposed. The key to a successful and feasible outcome is attributed to synergistically employing microfluidic-enabled patterning for noninvasive mechanical stimulation of single cells and total internal reflection fluorescence microscope (TIR-FM) for live single cell cytokine detection. The TIR-FM platform is based on a sandwich immunoassay, established for a sensitive detection of small molecules such as cytokines [41]. Combining microfluidics with TIR-FM provides a tool to study correlations between physiological shear stress applied on single astrocyte cells and the resulting secreted cytokine concentration. Ultimately, our microfluidic/TIR-FM biosensor allows for improved device design for the next-generation medical devices.

In this study, we developed a unique and feasible platform by combining a microfluidic shear device chip (MSDC) with TIRFM to better understand shear stress-dependent inflammatory astrocyte activation, through real-time quantitative analysis and direct spatial-temporal mapping of secreted cytokines upon shear stress at the single-cell level. Single-cell methods provide unprecedented, detailed information about dynamic behavior of complex spatiotemporal distributions of cytokines as well as transient and rare cellular states which complement bulk assays. Here, by using our TIR-FM/MSDC biosensor we examined the correlations between physiological shear stress greater than 0.5 dyne/cm^2 applied on single astrocytes and the resulting IL-6 cytokine secretion to answer our question of whether shear stress significantly accelerates astrocyte activation on the CSF shunt surface. The answer will dramatically change our perspective of treatment of hydrocephalus, and sheds light on other chronically indwelling probes in the brain.

3.2.1. TIR-FM and single cell cytokine secretion

Total internal reflection fluorescence microscope (TIR-FM) is an advanced imaging technique that allows for small (less than 100nm thick) regions of a sample to be examined while excluding noise from the rest of the sample. TIR-FM is based on the phenomenon known as the evanescent wave. When excitation light is shone on an interface between two different media at an angle greater than what is known as the critical angle, the excitation light undergoes total internal reflection and is not transmitted into the sample. However, at the critical angle a small exponentially decaying light called the evanescent wave does get transmitted into the sample. This wave typically penetrates less than 100 nm

of the sample. The part of the sample inside this evanescent wave region is then viewed through the microscope. By only illuminating the first 100 nm of a sample, the TIR-FM system achieves the high signal-to-noise ratio necessary for creating precise biological images with very high sensitivity and wide temporal resolution. This selective excitation also reduces photobleaching of fluorophores in solution and prevents harmful light damage when imaging live cells [42].

3.2.2. Real-time spatial-temporal single-cell cytokine detection

Conventional methods for cytokine quantification are immunoassay-based techniques such as enzyme-linked immunosorbent assay (ELISA) and bead-based immunoassay using a flow cytometer or plate reader which requires multiple washing steps. The minimum assay time (the minimum time between sampling and detection) is more than an hour, therefore not ideal for acute inflammatory disease settings. Therefore, enforcing limitations on personalized immunomodulatory therapy, where suitable cytokine-blockade drugs are to be delivered at a right dose in a timely manner. Thus, creating a gap between the demand for rapid, sensitive assays of cytokine levels and the assay techniques for a fine-tuned immune control.

In literature there are many cytokine detection methods [43]–[46], however not in real-time and for single-cells. Recent advances in microfluidics and imaging techniques have brought together advances in biosensing for excellent sensitivity in detecting biomolecules. Integrated in a microfluidic system, these biosensors allow for high throughput detection yielding a large surface-to-volume ratio in a small-volume while also reducing the

diffusion distance of the molecules leading to rapid detection resulting from enhanced biomolecule–sensor interactions. Real-time observation of cellular cytokine secretion in response to stimulation mimicking a disease state provides a precise determination of the cellular behavior. The significance of the TIR-FM cytokine detection assay is summarized as:

1. The PDMS surface replicates the shunt surface.
2. Real-time, spatial-temporal mapping of cytokine secretion.
3. High-throughput multiplex cytokine detection.
4. Quantity and quality: multidirectional/synaptic.
5. Non-invasive as immobilizing and labelling target molecules is in the extracellular space: no tagged molecules inside the cell.
6. High signal to noise ratio for cytokines with small size.
7. Dynamic and kinetic with no lag between secretion and detection.
8. High time resolution for the initial stages of continuous/burst cytokine secretion from cells.
9. Quantifying at the same time as observation for cell phenotype/morphological changes/viability.
10. Maintenance of cellular physiology without prolonged isolation.
11. Simultaneous detection of adhesion molecules or other intracellular processes that occur at the time of cytokine secretion (differences among adhesion molecules and surface distribution altered by mechanical stimulation of the surface in live cells).

3.3. Materials and methods

3.3.1. TIR-FM/MSDC biosensor reagents

Capture and detection antibodies used for sandwich immunoassays for human IL-6 monoclonal antibody (clone 6708; MAB206) and human IL-6 biotinylated affinity purified polyclonal antibody (BAF206) were purchased from R&D Systems. CF660R streptavidin was purchased from Biotium (29040; Hayward, CA, USA). Human astrocyte cells were purchased from ScienCell Research Laboratories (Catalog no. 1800) commercial cell lines. FN from human plasma was purchased from sigma. Sylgard-184 elastomer and curing agents were purchased from Dow Corning. Human tumor necrosis factor-α (hTNF-α) no. 8902 and human interleukin-1β (hIL-1β) no. 8900 were purchased from Cell Signaling Technology.

3.3.2. TIR-FM/MSDC biosensor setup

Astrocytes cells were prepared in a CO_2 incubator at 37 °C in a humidified atmosphere with 5% CO_2. The cells were incubated in astrocyte medium containing 2% FBS (ScienCell Instruction). To permit phenotypic maturation of astrocytes, astrocytes were used in all experiments at passage 3. Astrocytes were tested for presence of glial fibrillary acidic protein, of which all cells are positive in the culture conditions described. The day before TIR-FM experiments astrocytes cells at a low concentration were flowed into the MSDC at 0.5 µl/min for 10 min and cultured overnight. Cell culture medium was flowed at 0.5 µl/min to remove the suspension cell before stressing them. Different flow rates were applied with the detection medium containing CF-labeled detection antibody

(30 nM), TNF-α (100 ng/ml) and IL-1β (2 ng/ml). The cells were monitored before and after stimulation. For imaging, the coverslip chamber containing cells were transferred to a 37 °C pre-warmed microscope stage. TIR-FM imaging was performed using a Nikon TiE-Perfect Focus System (PFS) microscope equipped with an Apochrmomat 100× objective (NA 1.49), a sCMOS camera (Flash 4.0; Hamamatsu Photonics, Japan) and a laser launch controlled by an acousto-optical tunable filter (AOTF). Image acquisition was controlled by ImageJ Micro-manager software (NIH). The 640 nm channel time-lapse image series were acquired by using 200 ms exposure at 5 s interval for 120 min. Single astrocyte cells were identified and localized in individual image frames [47], [48].

3.3.3. Detection medium

Detection antibody labeled with biotin was coupled with CF-labeled streptavidin at 1:10 molar ratios at room temperature in the dark for 3 h. Unoccupied sites on streptavidin were blocked with excess dPEG4-biotin acid (10199; Quanta BioDesign, Ltd., Powell, OH, USA). Unconjugated streptavidin and dPEG4-biotin were removed by ultrafiltration (Amicon Ultra-0.5, 100 kDa; Merck Millipore, Billerica, MA, USA). The detection media contained prepared CF-labeled detection antibody (30 nM), TNF-α (100 ng/ml), and IL-1β (2 ng/ml).

3.3.4. Microfluidic shear device chip (MSDC)

Microfluidic devices enhance the reaction speed of reagents with a confined volume and provide conditions suitable for detecting low concentrations of small molecules and

the chance for the biomolecules to meet with target receptors on the sensor, reducing the binding assay time. The microfluidic device creates a short cell-to-sensor distance positioning cytokines near target receptors on the sensor surface. Therefore, the diffusion time of cytokines to the sensing surface is reduced for high throughput signal sensing.

Standard soft lithography techniques were used to create the silicon master mold from which polydimethylsiloxane (PDMS) stamps were made. PDMS stamps were prepared by mixing Sylgard-184 elastomer and curing agents at a ratio of 10:1 (w/v), casting over the mold, and curing at 60 °C overnight. The PDMS stamp and glass coverslip were permanently bonded together after the contact surfaces between them were plasma-treated. PDMS-coated coverslips were prepared by spin-coating a layer of PDMS diluted in hexane (1:20) at 5000 rpm for 2 min [47]. About 40 μg/ml FN was added to the PDMS-coated coverslips and glass coverslips then incubated for 1 h at room temperature. A 100 μl mixture of capture antibodies (100 μg/ml) was loaded onto the PDMS-coated coverslips and glass coverslips. The surface was blocked with Pierce protein-free blocking buffers.

3.3.5. COMSOL simulations of shear stress in microchannels

In a microfluidic device, physical shear stress can simply be regulated by fluid flow induction for a laminar flow behavior. This concept is based on the laminar flow Navier-Stokes theory, since the flow in the microfluidic channel is laminar, Newtonian flow, and incompressible. The laminar shear stress in the microfluidic channel can be estimated as:

$$\tau_{wall} = \frac{6\mu Q}{wh^2}$$

in the unit of dyne/cm^2 (1 Pascal = 10 dyne/cm^2), μ is the fluid dynamic viscosity, Q is the volumetric flow rate, h is the channel height, and w is channel width. Thus, the mechanical shear stress generated on the cell in the channel is proportionally relative to the flow rate. Small dimensions associated with micrometer-sized channels ensure laminar flow even at very high linear fluid rates. COMSOL simulations were conducted to demonstrate that the microchannels experience a uniform shear stress distribution.

In this study, the design of the microfluidic shear devices was motivated by the experimental objective of four microfluidic channels with different width to provide a multiplex culture platform to measure four different shear stress stimulation on astrocytes. However, to eliminate any geometry-dependent factor, the data collected in this study are only for the widest channel of 1000 μm width. Therefore, the volumetric flow rate Q changed for different shear stress stimulations.

3.3.6. ELISpot

The enzyme-linked immunospot (ELISpot) assay quantifies cytokine-secreting cells at the single-cell level. The assay is highly sensitive as the cytokines secreted are immediately captured. After cells are cultured on a specific capture antibody coated surface the number of cytokines secreted from single cells in the presence of stimuli will be captured and quantified using a detection antibody like the ELISA assay.

Simultaneous ELISpot assay was performed with the same cell preparations and the same shear stress conditions as the MSDC. The chip surface was coated with antibodies, and the cytokines secreted by astrocytes were trapped on the surface around the

cell. Binding of the cytokine to the specific antibodies formed fluorescent signals around the cell, which were acquired using confocal microscopy: Olympus-IX81 fluorescence microscope with spinning disk confocal scanner unit (CSU-X1; Yokogawa, Japan), EMCCD camera (iXon X3; Andor, South Windsor, CT), 60× objective (NA = 1.42).

3.3.7. Statistics and reproducibility

GraphPad Prism 8 was applied for data analysis. To statistically define data normality the Anderson–Darling test was used. After homoscedasticity and QQ plots were created, a two-way repeat measure ANOVA was used with an alpha value set to 0.05 with sphericity assumed. Sidak's multiple comparisons test was performed to observe post hoc multiple comparisons.

For TIR-FM and ELISpot, independent experiments were performed on three different devices (n = 3) per substrate (glass and PDMS). For ELISpot, the number of replicates for each data point were at least five cells measured (n = 5), provided in the corresponding figure captions.

3.4. Results and discussion

3.4.1. TIR-FM/MSDC biosensor along the shunt hole/CSF interface

Along the shunt hole/CSF interface, astrocytes are simultaneously exposed to fluid flow shear stress and TNF-α/IL-1β cytokine stimulation secreted from activated microglia/macrophages on the shunt surface [12]. Based on reports, shear stress has less effect on microglia/macrophages, but a direct stimulation effect on astrocytes. Co-

stimulation with TNF-α and IL-1β induces a proliferative reactive astrocyte phenotype called A2 [49], [50], that secrete IL-6 cytokines. IL-6 activates astrocyte proliferation by a positive feed-forward loop, further activating local astrocytes implicated in the induction of glial scar formation (Figure 3.1a). The unique TIR-FM/MSDC biosensor effectively reproduces the brain tissue response by applying physiological shear stress on single astrocyte cells and providing quantitative data on spatial secretion of cytokines in real-time by detecting formation of cytokine sandwich immunocomplex immediately following astrocyte secretion. The anti-cytokine capture antibody immobilized on the microchannel surface, onto which secreted cytokine and fluorescently labeled detection antibody is bound, form the sandwich immunocomplex (Figure 3.1b). In a microfluidic device, physiological shear stress can be created by fluid flow induction at a predetermined rate, in the presence of TNF-α/IL-1β to determine the influence of shear stress on specific astrocyte phenotypes. In this study, four microfluidic channels with different widths were designed to provide a multiplex culture platform to measure four different shear stress stimulations on astrocytes (Figure 3.2a). COMSOL simulations were conducted to demonstrate that the microchannels experience a uniform shear stress distribution, and thus the astrocytes are subject to a uniform shear stress (Figure 3.2b). Given that computational fluid dynamics simulations have shown that in CSF shunts, the wall shear stress at the proximal holes (holes located furthest from the tip) is larger than 0.5 dyne/cm^2, in this study high uniform wall shear stress of more than 0.5 dyne/cm^2 across the microchannel's surface is maintained. The control as low shear stress is less than 0.05 dyne/cm^2 wall shear stress

across the microchannel's surface, which is less than one tenth of the wall shear stress that induced cytokine secretion from astrocytes.

We know that the initial phase of the FBR is blood-device interactions, which occurs immediately upon implantation caused by vasculature or blood–brain barrier (BBB) disruption, resulting in the influx of serum proteins and their nonspecific adsorption to the device surface. Thus, in this study for an appropriate representation of the in vivo occurrence of inflammatory response on silicone CSF shunts, polydimethylsiloxane (PDMS) coated glass substrates were selected with nonspecific adsorptions of blood proteins, such as fibronectin (FN).

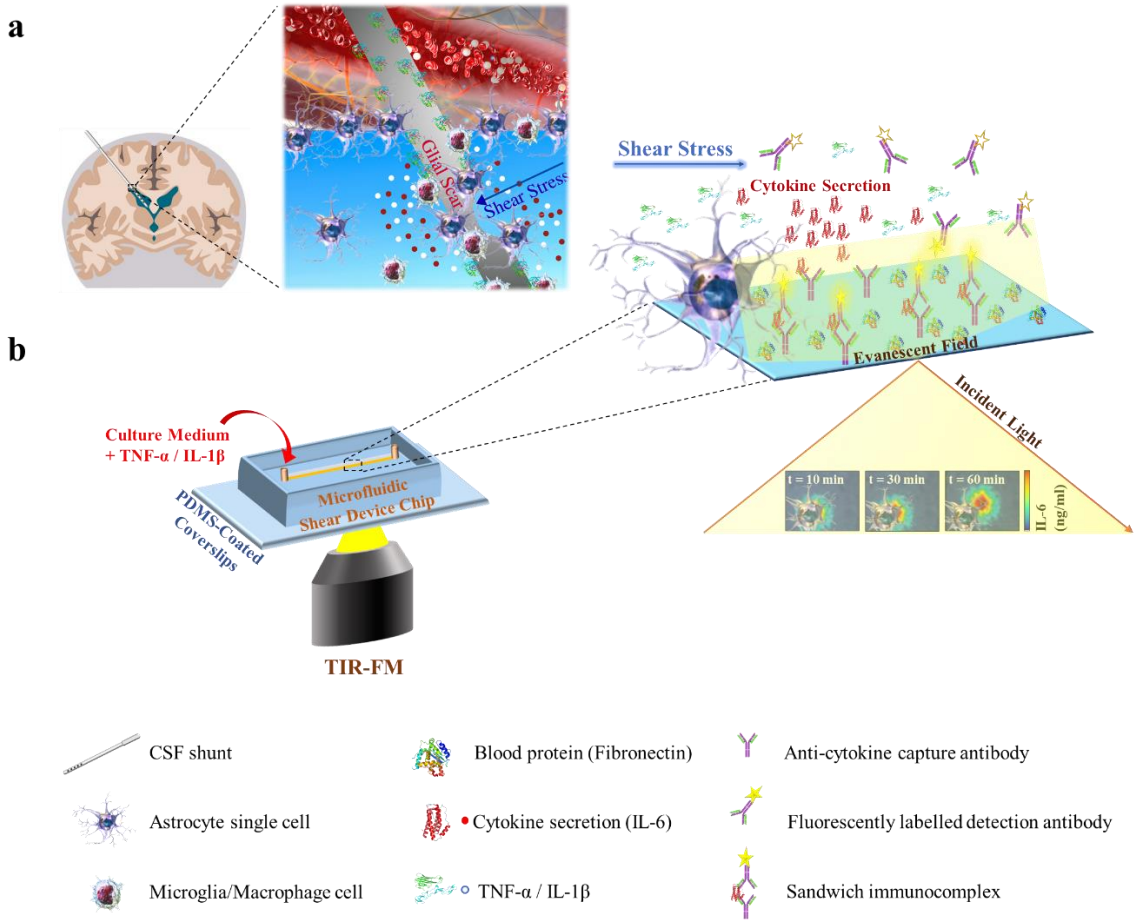

Figure 3.1. Real-time spatial monitoring of live single-cell cytokine secretion assay platform for reproducing the physiological response along the shunt hole/CSF interface. Schematic of the (a) inflammatory FBR along the shunt hole/CSF interface (b) TIR-FM/MSDC biosensor: by taking advantage of near-field excitation in TIR-FM, target cytokines in each MSDC microchannel are quantified by detecting formation of cytokine sandwich immunocomplex immediately following single-cell secretion. The anti-cytokine capture antibody immobilized on the microchannel surface, onto which secreted cytokine and fluorescently labeled detection antibody is bound, form the sandwich immunocomplex. The detection strategy presents an advantage in its non-invasive quantification by immobilizing and labeling target molecules in the extracellular space.

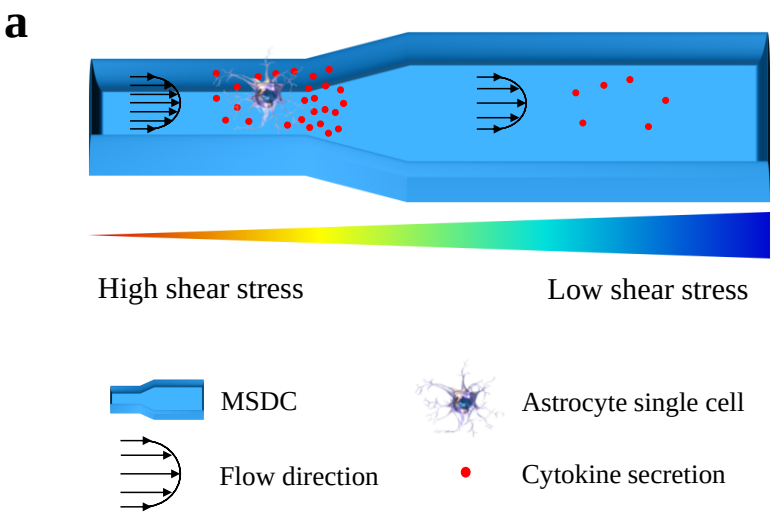

Figure 3.2. Multiplex high-throughput microfluidic device for uniform shear stress stimulation of cells.
(a) Schematic of the MSDC design with different widths to provide a multiplex culture platform to measure different shear stress stimulations on cells. The microchannel with a smaller width and a higher fluid flow shear stress presents higher cytokine secretion from cells. (b) COMSOL simulations of flow in the microchannels predicted relatively uniform wall shear stress values across cell adhesion areas for all TIR-FM analysis. A flow rate of about 10 μl/min generates more than 0.5 dyne/cm^2 of uniform wall shear stress across the widest rectangular microchannel's surface of 1000 μm width.

3.4.2. Performance evaluation of the TIR-FM/MSDC biosensor

Experimental validation of the TIR-FM/MSDC platform was carried out by introducing different concentrations of cytokine into microchannels, mimicking cytokine secretion from a single-cell, and quantifying the amount of fluorescence signals. Fluorescence signals increased immediately after introduction of IL-6, indicating that the introduced IL-6 was instantly captured by antibody in the microchannel. Fluorescence increases with an increase in IL-6 concentration on both glass and PDMS substrates (Figure 3.3a), indicative of a successful platform. The capture ratio of the TIR-FM/MSDC biosensor depends upon variables such as the height of the cytokine release point (which determines the probability of the cytokine encountering the capture antibody). Therefore, the assay platform developed in this study is proficient for in situ detection of the onset of cytokine secretion from single cells at high temporal resolution in a sensitive and selective manner, while also providing semi-quantitative data on secreted cytokines (Figure 3.3b).

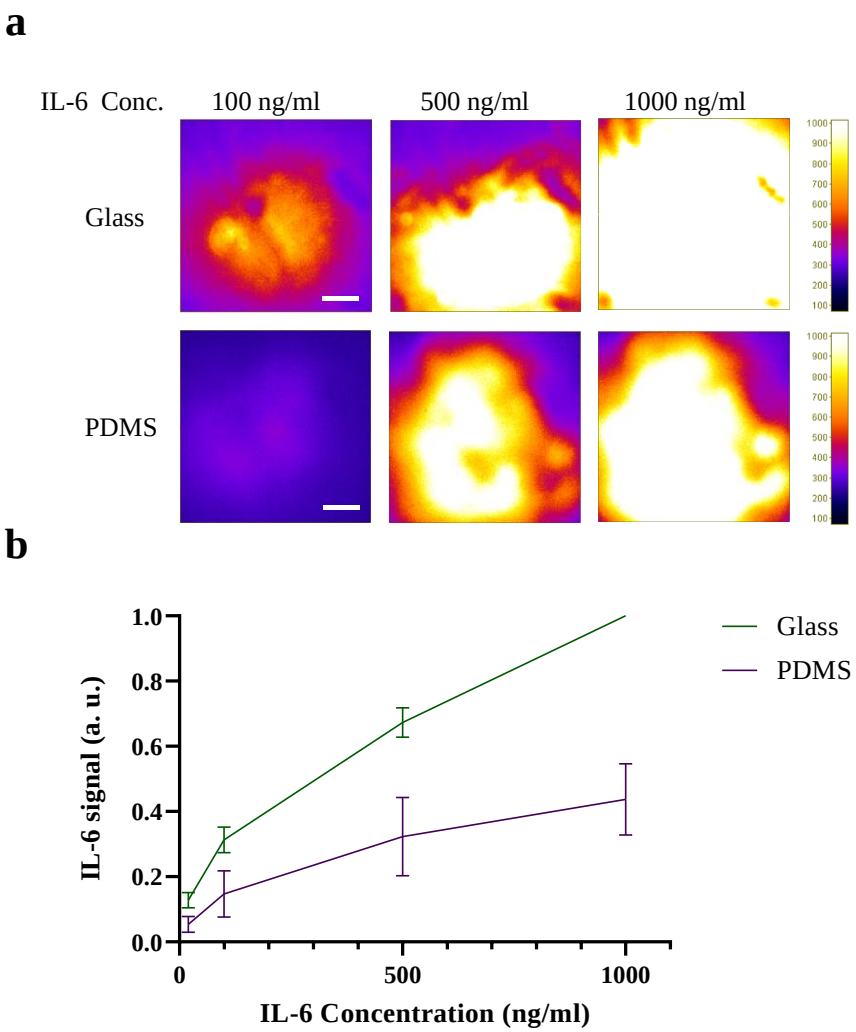

Figure 3.3. Standard curve for performance evaluation of the TIR-FM/MSDC biosensor. (a) Representative images of developed fluorescence signals obtained after introducing different concentrations of IL-6. An increase in fluorescence signal was observed after an increase in IL-6 concentration. (b) The average intensity of the IL-6 quantified values from (a). Glass substrates (green) were more efficient at binding IL-6 compared to PDMS substrates (purple). The results are represented as individual data points in the plots and the solid line denotes the average value. Data were normalized via dividing by the maximum value to bring all the measured values in the dataset to the same metric scale. Independent experiments were performed on three different devices (n = 3) per substrate. Scale bars represent 10 μm.

3.4.3. TIR-FM/MSDC biosensor for shear-cytokine activation of astrocytes

Along the shunt hole/CSF interface, astrocytes are simultaneously exposed to fluid flow shear stress and TNF-α/IL-1β cytokine stimulation (shear-cytokine activation). To answer our question of whether under physiological conditions shear stress significantly accelerates astrocyte activation on the CSF shunt surface, the TIR-FM/MSDC biosensor was employed. Time- and space-resolved observation under simultaneous fluid flow shear stress and TNF-α/IL-1β cytokine activation of single human astrocytes revealed a significant increase in IL-6 secretion under high shear stress compared to low shear stress controls (Figure 3.4). Initially ($t = 10$ min) when cytokine stimulation of astrocytes has not started, shear only stimulated astrocytes on glass substrates for both low and high shear stress had no IL-6 secretion. However, as time increases ($t > 30$ min) astrocytes under high shear-cytokine activation resulted in significantly ($p = 0.0015$) higher levels of IL-6 secretion compared to low shear-cytokine activation (Figure 3.4a, d). Under low shear stress, IL-6 multidirectional diffusion in space around the cell is detected. However, under high shear stress, IL-6 distribution in space away from the cell is observed (Figure 3.4a, b). The rising curve of IL-6 secretion from shear-cytokine activated astrocytes, indicative of an increase in IL-6 concentration, occurred as a concave-down function, suggesting IL-6 was secreted in a burst release pattern rather than continuous secretion of IL-6, based on reports [41] (Figure 3.4d). Real-time monitoring of cells over time ensured that astrocytes were not detached from the surface, under high shear stress. Via this unique assay platform, simultaneous dynamic cellular states for live single cells could also be observed such as a change in astrocyte phenotype from a resting to a reactive form under shear-cytokine

activation, characterized by horizontally swollen bodies (Figure 3.4c). Swelling of reactive astrocytes was quantified as the increase in cross-sectional area relative to the resting astrocytes. On PDMS substrates, similar results for shear stress were observed, with high and low shear created a significant difference in the IL-6 secretion after 30 min of activation ($p < 0.031$). However, astrocytes on hydrophobic PDMS substrates, initially displayed higher activation of IL-6 secretion compared to hydrophilic glass substrates under high shear stress. Together, these data provide evidence that astrocytes directly sense the mechanical stress and translate it into chemical messages of rapid increase in IL-6 cytokine secretion.

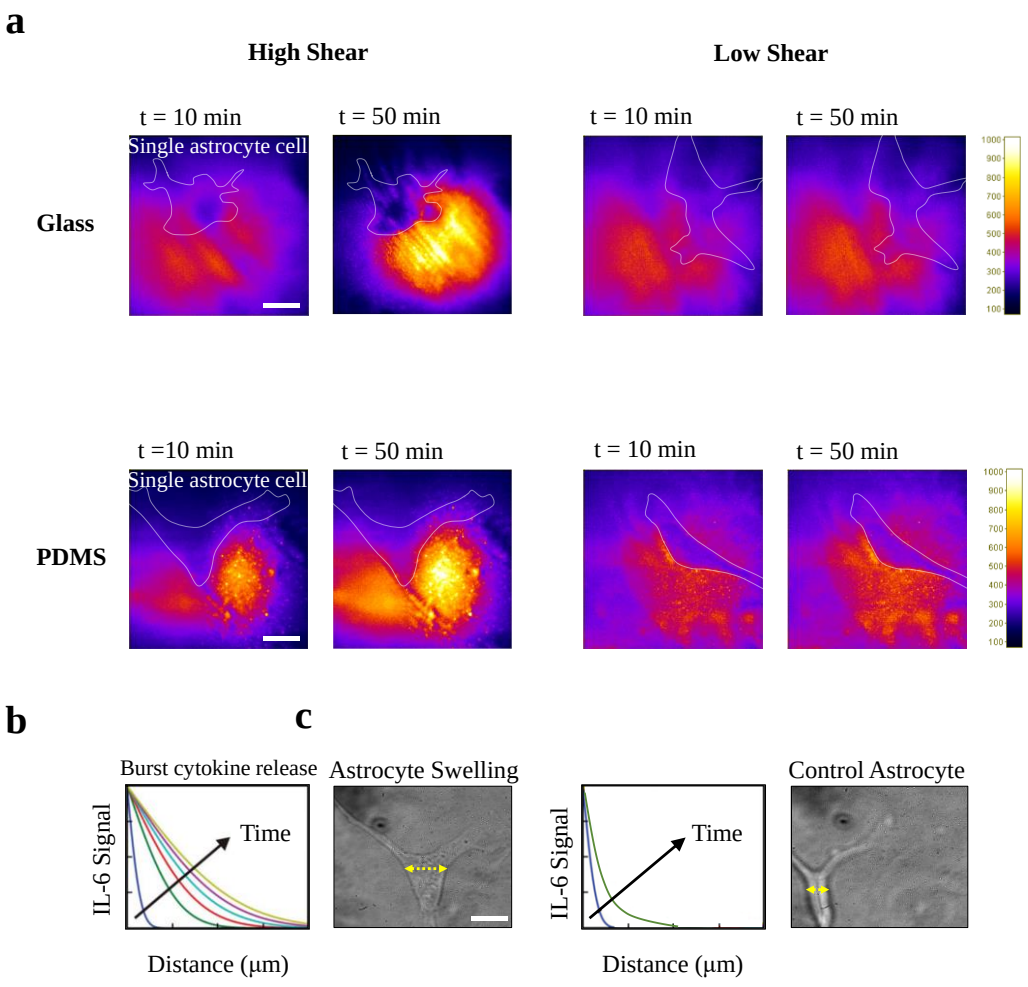
a
High Shear
Low Shear
t = 10 min
t = 50 min
t = 10 min
t = 50 min
Glass
Single astrocyte cell
t =10 min
t = 50 min
t = 10 min
t = 50 min
PDMS
Single astrocyte cell
b
c
Burst cytokine release
Astrocyte Swelling
Control Astrocyte
IL-6 Signal
Time
Distance (μm)
IL-6 Signal
Time
Distance (μm)

d

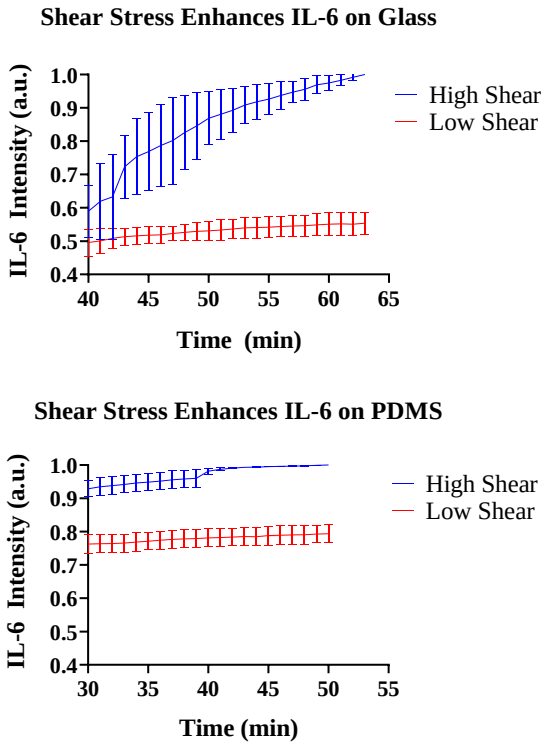

Figure 3.4. Spatial-temporal mapping of secreted cytokines from single astrocyte cells upon shear stress on different substrates.
(a) Quantitative spatial temporal resolution mapping of IL-6 concentration under low and high shear stress at time 10 and 50 min, on glass and PDMS substrates. (b) Time course of the average intensity of IL-6 signals under low and high shear. The results are represented as individual data points in the plots and the solid line denotes the average value. Data were normalized via dividing by the maximum value to bring all the measured values in the dataset to the same metric scale. Independent experiments were performed on three different devices (n = 3) per substrate. (c) Representative measures depicting spatial-temporal mapping of IL-6 signal dependent on distance from astrocytes for a duration of 50 min. (d) Brightfield image of resting and high shear-cytokine activated single astrocyte cell, characterized by horizontally swollen bodies. The cross-sectional area was calculated using a line drawn to measure the diameter of astrocyte boundary. Single astrocyte cells were identified and localized in individual image frames. Scale bars represent 10 μm.

In this study simultaneous shear-cytokine activation of astrocytes was performed, showing significantly higher levels of IL-6 secretion under higher shear stress compared to lower shear stress. Initially, shear-only stimulated astrocytes resulted in no IL-6 secretion on glass substrates for both low and high shear stress, indicating that shear stress alone does no induce astrocyte activation. PDMS substrates show a very minimal increase of IL-6 signal at time zero. However, as time increases astrocytes under high shear stress resulted in significantly higher levels of IL-6 secretion on both substrates. The simultaneous effect of shear-cytokine activation had a strong effect on IL-6 secretion, higher than only cytokine (TNF-α/IL-1β) activation observed for low shear stress. These findings are consistent with other reports [51]–[53]. Our results verify that along the shunts proximal hole (hole located furthest from the tip) with the highest shear stress, astrocytes are significantly activated to secret IL-6. Since IL-6 activates astrocyte proliferation by a positive feed-forward loop, local astrocytes are also significantly activated and proliferate to form the glial scar on the shunts proximal hole [54], leading to high shunt device failure rates. Moreover, recent long-term in vivo data collected in our lab indicate astrocyte markers in obstructive masses on shunts to be co-localized with proliferative markers, indicating that astrocytes are active on the shunt surface: they produce inflammatory cytokine IL-6 and proliferate.

Single astrocyte cells were identified and localized in individual image frames at least 100 μm apart from other astrocytes. Since the distance over which cytokine-mediated communication happens effectively is far less than 100 μm, and cytokine signaling are limited to small distances of only a few cell diameters [55]–[57], substantiates that the IL-

6 secretion detected is only from the identified single astrocyte cell. To observe simultaneous dynamic cellular states under shear-cytokine activation, future work will expand on the degree of cell reactivity by quantifying astrocyte processes directionality and bifurcation number.

Shear-cytokine activation of astrocytes was simultaneously performed using the ELISpot assay on a second prepared MSDC. The same procedure is used as TIR-FM experiments, with the difference of detecting signals for IL-6 secretion from a population of astrocytes attached on the surface, instead of single astrocytes (Figure 3.5a). In accordance with our TIR-FM data, ELISpot data confirm that under high shear stress, despite less cell attachment on both glass and PDMS substrates compared to low shear stress, a significant ($p = 0.0056$ and $p = 0.0005$, respectively) increase in IL-6 secretion was detected (Figure 3.5b).

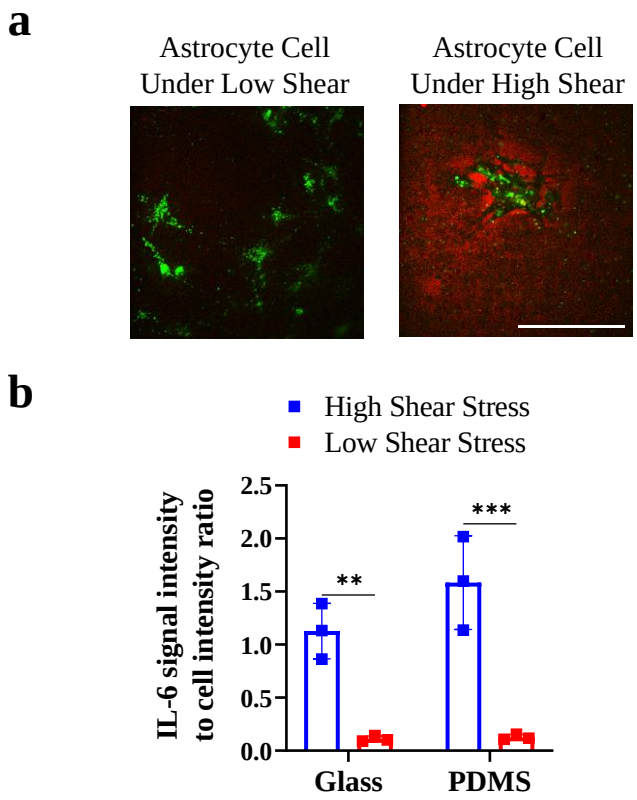

Figure 3.5. ELISpot population analysis of astrocyte under low and high shear stress on different substrates.
(a) Representative fluorescence image for glass substrate qualitatively depicting IL-6 signal (red) distribution merged with astrocyte signal (green), and (b) IL-6 signal intensity to cell signal intensity ratio. After shear-cytokine activation of astrocyte, astrocytes were stained with DiO lipophilic membrane labeling dyes. Each data point denotes an average value for n = 5 cells measured. Intensity values were normalized for the number of cells present. Independent experiments were performed on three different devices (n = 3) per substrate. The results are represented as mean ± SD in the plots. Scale bar represents 100 μm. The p values ** and *** denote p = 0.0056 and p = 0.0005.

ELISpot data confirm that under higher shear stress, despite less cell attachment to the surface, a significant increase in IL-6 secretion is detected. This is strongly in accordance with other reports, which indicate a necessity for control of the degree of inflammatory cell activation for considerable improvement of device performance within

the brain, in contrast to the general implant failure of reduced cell adhesion on the device surface in vivo [26], [58]–[60]. Our results present a proof of concept that to have maximal impact, strategies should implement a focus on attenuating the initial inflammatory cell activation instead of only focusing on reducing cell adhesion on the device surface. Such strategies include decreasing shear activation as a primary cause of device failure, and directly antagonizing the accumulation of pro-inflammatory cytokines via targeted therapeutic for TNF-α and IL-6.

One advantage of our platform is the direct effect of surface property on the degree of astrocyte activation under physiological shear-cytokine activation. Under conditions of high shear stress, astrocytes on hydrophobic PDMS substrates resulted in higher IL-6 secretion compared to hydrophilic glass substrates, possibly due to cell spreading and contact between the attached cells and ligand adsorption on different surfaces. Furthermore, ELISpot data confirm that under low shear stress, there is nearly no change in the degree of astrocyte activation on hydrophobic/hydrophilic surfaces, indicating the high impact of shear activation on implant failure.

Considering that fluorescence signals for IL-6 detection on PDMS substrates were lower than on glass substrates for the generation of the standard curve (Figure 3.3), we expect data are underestimating the degree of astrocyte activation on PDMS (Figure 3.4). That is, under high shear stress, we expect the addition of cells to generate further astrocyte activation on PDMS substrates.

3.4.4. Shear-cytokine activation of astrocytes on FN-coated substrates

The unique real-time feature of our platform enables early cytokine activation detection of cells, for an accurate com prehension of earlier events in interfacing technology, leading to cumulative enhancements. Time- and space-resolved observation under simultaneous fluid flow shear stress and TNF-a/IL-1ß cytokine stimulation of single human astrocytes on FN-coated PDMS/glass substrates strikingly revealed astrocyte activation and high IL-6 signals at time zero, indicating that astrocytes had already been extremely activated, and had already released IL-6 on FN-coated substrates before shear-cytokine activation. However, the identical burst release pattern of IL-6 secretion is also observed under high shear stress for FN-coated substrates in time. The degree of astrocyte activation differs significantly on FN-coated hydrophobic/hydrophilic surfaces (Figure 3.6a). ELISpot data confirm the results obtained from the TIR-FM/MSDC biosensor. (Figure 3.6b).

a

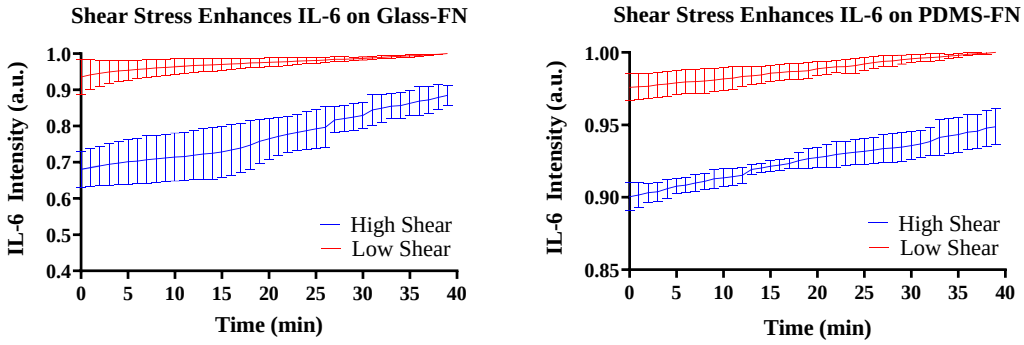

b

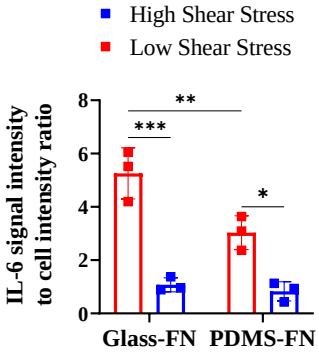

Figure 3.6. Fibronectin activation of astrocytes on different surfaces.
(a) Time course of the average intensity of IL-6 signals under low and high shear stress for glass and PDMS substrates. The results are represented as individual data points in the plots and the solid line denotes the average value. Data were normalized via dividing by the maximum value to bring all the measured values in the dataset to the same metric scale. Independent experiments were performed on three different devices (n =3) per substrate. (b) ELISpot population analysis of astrocyte under low and high shear stress on glass and PDMS substrates characterized as: IL-6 signal intensity to cell signal intensity ratio. Each data point denotes an average value for n =5 cells measured. Intensity values were normalized for the number of cells present. Independent experiments were performed on three different devices (n = 3) per substrate. The results are represented as mean ± SD in the plots. The p values *, **, and *** denote p = 0.0102, p = 0.0095, and p = 0.0002.

The unique real-time feature of our platform enables early cytokine activation detection of cells, to measure earlier events of disease progression. To highlight the importance, we observed that FN-coated PDMS/glass substrates result in high levels of IL-6 signals, at time zero, indicating that FN alone extremely activates astrocytes to secret IL-6. Such information is not obtainable by other traditional techniques. FN participates in converting quiescent astrocytes to a proliferating A2 phenotype in glial scars [61], [62]. These findings are consistent with other reports, indicating FN increases cell activation, which leads to differences in protein expressions [63]–[65]. Under high shear stress the burst release pattern of IL-6 secretion is observed for FN coated substrates, once more indicating the impact of shear stress activation. ELISpot data confirm the results obtained from the TIR-FM/MSDC biosensor. Also, of interest is the degree of astrocyte activation as it differs significantly on FN coated hydrophobic/hydrophilic surfaces. Since PDMS substrates without FN already show a minimal increase of IL-6 signal and astrocyte activation at time zero, PDMS substrates with FN show less effect on astrocyte activation compared to glass substrates with FN.

Therefore, since an arm of shunt obstruction is arguably originated from single astrocytes shed into the CSF, we can assume that shear stress activates these astrocytes to secret cytokines. This would induce exaggerated proliferation in astrocytes as they bind to the FN adsorbed on shunt surfaces [66]. Even so, if we assume shunt obstruction also originates from astrocytes migrating into the shunt holes from the parenchyma or ventricular wall, these cells would be exposed to high shear stress and similarly release IL-6 for exaggerated proliferation [34]–[36].

Another advantage of real-time cytokine secretion dynamic in space is elucidating the chronological relationship between intracellular events by allowing simultaneous monitoring of a second cellular variable. For example, since cell adhesion increases as well with shear stress on astrocytes via intercellular adhesion molecule-1 (ICAM-1) ligation on astrocytes, and TNF-α and IL-1β mediate ICAM-1 induction via microglia/macrophages–astrocyte interaction in CNS injury [67]–[69], the TIR-FM/MSDC biosensor will allow for simultaneous visualization of ICAM-1 expression on astrocyte cells and cytokine secretion profiling under shear stress, and their chronological relationships.

A precise selection of astrocyte phenotype leads to a precise control of astrocyte activation. In a landmark study, Barres and colleagues identified two significantly different reactive astrocyte phenotype which they called A1 and A2 [50], [70]. The A1 neuroinflammatory astrocytes are induced by NF-κB signaling, whereas A2 scar-forming, proliferative astrocytes are induced by STAT3-mediated signaling [54], [70]. Given that glial scar borders are formed by newly proliferated, elongated astrocytes via STAT3-dependent mechanisms, studies strongly suggest that the A2 reactive astrocyte phenotype is present during glial scar formation [50], [71], [72]. In this study, serum-cultured human astrocytes are used which based on reports express many of the A2 astrocyte genes [54], [73], since in vivo, quiescent astrocytes contact serum upon injury and blood-brain barrier (BBB) disruption [74]. Additionally, IL-6 signaling pathways are enhanced in A2 astrocyte phenotypes, and STAT3 is activated by IL-6 implicated in the induction of glial scar formation on the device surface [54], [75]. Co-stimulation with TNF-α and IL-1β induces A2 reactive astrocyte phenotype [49]. Interestingly, expression of TNF-α, IL-1β and IL-6,

is rapidly upregulated in the injured CNS, and are observed right at the device-tissue interface corresponding to the location of activated microglia/macrophages and astrocytes [10], [12], [13], [26]. IL-6 promotes neuronal survival and neurite growth. These features are indications of the beneficial roles of IL-6 in repair and modulation of inflammation in the CNS. However, the overproduction of IL-6 is associated with glial scar formation, and periventricular white matter (where neuroinflammation occurs) injury due to increased CSF concentrations of IL-6 [76]. Thus, a careful inflammatory balance of IL-6 is necessary for proper repair. Inhibition of both IL-6 and IL-6r by antibody neutralization reduces damage to surrounding brain parenchyma as a result of bystander effects of increased CSF cytokine levels [77].

Our platform provides a comprehensive picture of the real-time single-cell modes of multiplex cytokine secretion profiles in space around the cell: one directional/multidirectional, autocrine/paracrine, continuous/concentrated burst (Table 1). Cells release some cytokines in one direction to impart synaptic cell-to-cell communication and others multidirectional to establish chemokine gradients and recruit inflammatory cells. For example, to prevent shunt obstruction, other than manipulating the shunt geometry, drug therapy is also used for inhibition of cytokines and therefore inhibition of scar formation [78]. However, cytokines that are secreted in one direction may be less accessible to blocking agents and therefore more difficult to target than multidirectional cytokine secretions [43]. Therefore, spatiotemporally determining cytokine secretion profiles in response to shear forces using the TIR-FM/MSDC biosensor is critical for predictive models of immune responses to prevent cell activation. Since astrocytes express

cytokines in a threshold dose- and time-dependent fashion, parameters for a controlled delivery could also be determined, specifically, the onset point, the dosage, and the duration. Ultimately, our platform allows for improved device design together with drug therapies for the better-quality of next-generation medical devices. For example, since IL-6 production is considered a downstream sequence related to TNF-α/IL-1β stimulation of cells, FDA-approved neutralizing monoclonal antibody therapies that inhibit human TNF-α, IL-1β, and the IL-1 receptor have been developed to decrease their activity [70], [78]–[80].

Table 1. Cytokine immunotherapy based on cell modes of cytokine secretion.

Cell Modes of Cytokine Secretion Space and Time Profiles Around the Cell	**Cytokine Immunotherapy** Predictive Models of Immune Responses to Cure Diseases
Burst / Continuous	- Time interval - Duration - Rate: molecules/min
Directionality	- Multidirectional - Synaptic (one direction)
Range of secretion (to prevent side effects)	- Low: only target cell - High: surrounding cells
Concentration of cytokine	Dosage of blocking drug

3.5. Directions for future applications

Although the brain tissue response (neuro-inflammation) is the main reason for chronic recording failure in neuroprosthetic devices, the exact mechanisms of failure require more investigation. Persistent inflammatory cell immunoreactivity accompanied

by a significant reduction in nerve cell bodies in the tissue immediately surrounding the implanted microelectrode is observed. However, in microelectrode stab controls persistent inflammatory cell immunoreactivity followed by neuronal loss was not detected. Indicating that the cell immunoreactivity is related to the foreign body response (FBR) and is not a result of the initial mechanical trauma after electrode implantation. In addition, explanted electrodes were covered with inflammatory immunoreactive cells that released MCP-1 and TNF-α, MMP 2 and 9. Still, studies should include concentration levels, half-lives, clearance rates or diffusivity. Thus, the new and key cause for chronic recording failure in neuroprosthetic devices that results in neuronal cell loss, is triggered by chronic inflammation and the persistent presence of motion-induced damage at the brain tissue interface. And is not the result of iatrogenic injury or BBB disruption and infiltrating blood products such as fibrinogen and plasma soluble fibronectin [81].

3.5.1. Device design to reduce motion-induced damage

Distributions for astrocyte released cytokines and neuroinflammatory response relate well with the neuroprosthetic designs despite device compliance. These findings indicate that geometry is a major contributing factor to the neuroinflammatory impact on surrounding neural tissue. To have maximal impact, studies suggest strategies that reduce the concentration of inflammatory and cytotoxic soluble factors to improve function. Thus, strategies aim at (1) reducing the number of reactive astrocytes, (2) reducing the reactive astrocyte phenotype, and (3) reducing the buildup of inflammatory and cytotoxic soluble factors secreted by astrocytes at the device interface.

CSF shunts removed for obstruction show occlusions to occur most often at the proximal holes (holes located furthest from the tip) with the highest flow [82]. These findings led to a recommendation that shunt geometry with a more uniform flow rate distribution through the shunt's inlet holes would decrease the obstruction specifically at the proximal inlet holes, in a way to reduce shunt failure rates. Therefore, as a solution a design comprising of reducing hole diameters from the distal to proximal end was established called the Rivulet (Medtronic Neurosurgery) shunt [4], [83]. However, shear stress will be higher in the proximal holes of these shunts. Based on fluid shear stress equation of $\tau = \mu\, du/dy$, where μ is dynamic viscosity, and du/dy is the gradient of velocity in the direction perpendicular to the flow, since the gradient viscosity of the decreasing hole diameters is higher, shear stress will be higher for the proximal holes. Based on our hypothesis and other reports of the correlation between increased shear stress along the shunt/CSF interface to result in increased occlusion [6], [34]–[36], [84], it is essential that the next-generation shunt design prototype attempts to decrease shear stress through all its holes or at best the proximal holes (Figure 3.7).

Another aspect to address is shunt size and geometry as it is relevant to the physical limitations of shunt design. Physical and surgical limitations of ventricular size, ventricular catheter environment, and ventricular catheter tip location to avoid hitting capillaries all have effect on the persistent high shunt failure rates particularly when dealing with pediatric populations. As we continue to design shunts, we will be working with neurosurgeons to accentuate lower shear stress according to the physical limitations of

ventricles. For example, exploring novel ways to improve the size of the holes and inner diameter for better compatibility with pediatric patients.

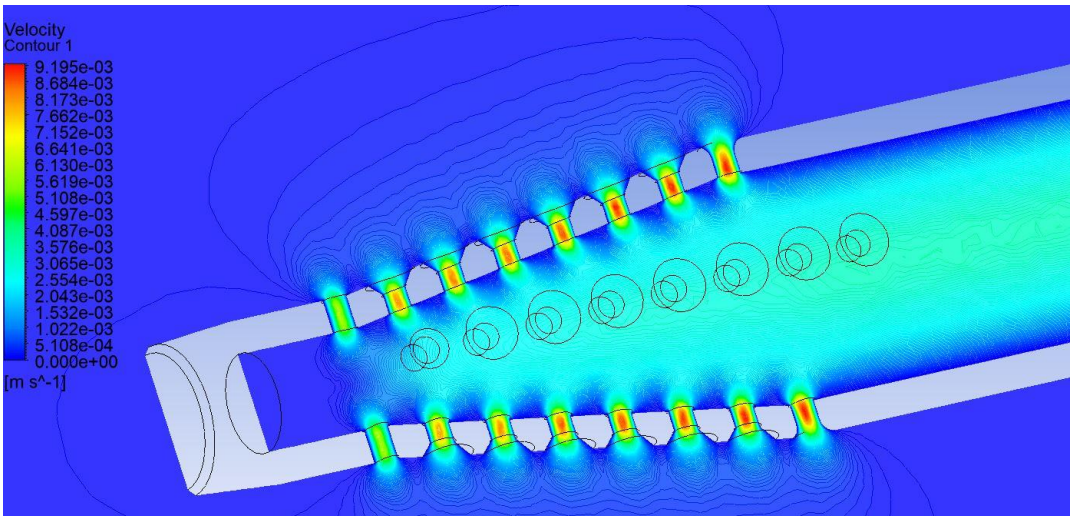

Figure 3.7. Mathematically design ventricular catheter, optimized to reduce astrocyte activation through shear reduction and flow redistribution.
Using ANSYS simulations of commercially available catheters, an optimized geometry was mathematically generated to maintain constant fluid velocity throughout the catheter. The shear is redistributed through all holes instead of the last 2 rows of holes.

For future work, it would be quite interesting to demonstrate the effects of a microfluidic shear device chip composed of a series of microchannels with varying diameter along their length (i.e., narrowing at various points along their length) to induce fluid flow shear stress [85]. Also, to establish the physiological conditions identified in hydrocephalus patients, astrocyte activation under different pulsation and flow rates, and CSF pressure over long periods of time provide as a potential area for future work. However, pulsation rate does not influence overall cell attachment in an acute, 20-hour period [35].

3.5.2. Cell-to-cell communication

Future studies include investigating the shear stress effect on single microglia/macrophage cells and single astrocyte–microglia/macrophage coculture system. Because both astrocytes and microglia/macrophage are the dominant cell types bound directly to shunt surfaces, understanding the complex connection between these cells will reveal mechanisms of various shunt failures and support the establishment of new shunt design and therapeutic approaches.

3.6. Conclusion

3.6.1. Shear stress the key driver of glial scar formation on implants

Device-induced injury events are not limited to the initial FBR failure mechanisms discussed above. Propagation of the immune response is due to continuous motion-induced damage at the device interface exacerbating the FBR, which in turn will severely compromise the device performance. In fact, motion-induced shear force is the primary cause of device failure aimed at significantly accelerating astrocyte activation, proliferation and attachment to device surfaces creating a compact glial scar [10], [14], [19], [26], [27], [86]. Based on literature, shear stress has a direct stimulation impact on astrocytes, but less impact on microglia/macrophages [14], [19]. Astrocytes directly sense mechanical stress and are activated to rapidly increase cytokine secretion that have been associated in the initiation of the glial scar formation.

3.6.2. Reproducing the physiological response to implantation in the brain

Mimicking the actual in vivo brain tissue response to implants requires a platform that is rationally designed and assisted by an improved knowledge of underlying biological processes discussed above. Our unique TIR-FM/MSDC platform effectively reproduces the physiological response by applying shear stress on single cells and providing quantitative data on spatial secretion of cytokines in real-time. In a microfluidic device, physiological shear stress can be simply created by fluid flow induction in either the absence or presence of TNF-α/IL-1β for a given time. Few studies have explored cytokine activation of astrocytes in the presence of physiological shear stress and even fewer with TNF-α/IL-1β and shear. Also, microfluidics for single-cell analysis offers higher throughput advantages over conventional petri-dish techniques of heterogenous responses and ensemble averaging. Single cell methods provide unprecedented, detailed information about dynamic behavior as well as transient and rare or unlikely cellular states which complement bulk assays. Complex spatiotemporal distributions of cytokines for an individual cell can also be revealed. The cytokine pathway is the best and most important measurable outcome for inflammatory cascades. Inflammatory cells at the brain-device interface communicate via cytokines to activate and recruit other inflammatory cells to the interface. Cytokine stimulation is a gateway for other gene products to be over- or under-expressed in the cascade, resulting in device failure. Therefore, the cytokine pathway is a starting point for mechanistic, thorough investigation of inflammation and device failure. Real-time cytokine secretion dynamics in space, serves as a powerful tool elucidating the chronological relationship between intracellular events by quantitative live cell imaging.

Thus, the unique TIR-FM/MSDC platform will one day be employed in real clinical applications for advancements in device interface technology.

Chapter 4. Neuroprosthetic device failure dependent on astrocyte phenotype?

4.1. Introduction to the study

Understanding the composition characteristics of the glial scar contributing to the high failure rate of neuroprosthetic devices implanted in the brain has been limited, to date, with the assessment of cells, tissue, and biomarkers obstructing the implant. However, there remains a critical knowledge gap in gene expression profiles of the obstructing cells. This first-time study investigates the phenotypic expression specific to astrocyte scarring from those cells on hydrocephalus shunt surfaces at the time of failure, aimed at the development of therapeutic approaches to target reactive astrocytes for improved functional outcome. Recent evidence has indicated that the tissue obstructing shunts is over 80% inflammatory, with a more exaggerated astrocytic response. To understand how to mitigate the astrocyte immune response to shunts, we performed gene expression profiling of the C3 and EMP1 genes to quantify if astrocytes were classically activated and pro-inflammatory (A1) or alternatively activated and anti-inflammatory (A2), respectively. Shunt catheters were removed from patients at the time of failure and categorized by obstructed vs non-obstructed shunts. RNAscope fluorescent in situ hybridization and quantitative PCR analysis of the C3 and EMP1 expressed genes revealed that a heterogeneous mixed population of both the A1 and A2 reactive phenotype exist on the shunt surface [50]. However, the number of A2 reactive astrocytes are significantly higher on obstructed shunts compared to A1 reactive astrocytes. ELISA data also confirmed higher levels of IL-6 for obstructed shunts involved in A2 reactive astrocyte proliferation and glial scar formation on the shunt surface. Since TNF-α and IL-1β propel resting

astrocytes into an A2 reactive state, by simply blocking the secretion or action of these cytokines, astrocyte activation and attachment on obstructing shunts could be inhibited.

4.2. Literature review

A deeper understanding of astrocyte phenotype leads to a more accurate interpretation of failure in chronically indwelling neuroprosthetics. In a recent world-renowned study, Barres and colleagues revealed two significantly different reactive astrocyte phenotype, A1 and A2 [50], [70]. The A1 reactive astrocytes produce large volumes of pro-inflammatory substances and neurotoxin that can induce neuronal death. The A2 reactive astrocytes upregulate anti-inflammatory substances and many neurotrophic factors, which promote survival and growth of neurons. The A1 neuroinflammatory astrocytes are induced by NF-κB signaling, whereas the A2 scar-forming, proliferative astrocytes are induced by STAT3-mediated signaling [54], [70]. Since glial scar borders are formed by newly proliferated astrocytes via STAT3-dependent methods, studies strongly suggest that the A2 reactive astrocyte phenotype is present during glial scar formation [50], [71], [72]. Furthermore, in vivo quiescent astrocytes that contact serum upon injury and BBB disruption, express many of the A2 reactive astrocyte genes. Primary purified cells grown in serum-free conditions have little-to-no expression of reactive transcripts, although those cultured in serum containing medium already greatly express many disease-associated reactive astrocyte transcripts [54], [73], [74] .

In the brain, TNF-α, IL-1α and C1q combined shift resting astrocytes into an A1 reactive state [70]. Co-stimulation with TNF-α and IL-1β induces the A2 reactive state with

neurosupportive characteristics [49]. In fact, TNF-α and IL-1β modulate the glial scar process by stimulating astrocyte IL-6 secretion [87]. IL-6 primarily activates astrocyte proliferation by a positive feed-forward loop, further activating local astrocytes to maintain the glial scar through self-maintaining methods. IL-6 signaling pathways, are enhanced in A2 reactive astrocytes, and STAT3 is activated by IL-6 [54], [75]. IL-6 is one of the primary causes of reactive astrocytes in the acute phase of disease, involved in improving neuronal survival and neurite growth [14]. Although, these properties are evidence of the beneficial roles of IL-6 in repair and alteration of inflammation in the CNS, the overproduction of IL-6 is associated with glial scar formation. Hence, a careful inflammatory balance of IL-6 is essential for proper repair. Inhibition of both IL-6 and IL-6r by antibody neutralization reduces glial scar formation on the implanted device and damage to the brain as a result of bystander effects of increased CSF cytokine levels [77].

Hydrocephalus is a devastating and costly disease. The most common treatment paradigm is surgical shunting of cerebrospinal fluid (CSF). However, shunts are plagued by unacceptably high failure rates (40% in the first year, 90% in the first ten years) [66], [88]–[90], and inflict a significant burden on patients, their families, and society. Understanding the root causes of shunt failure to design improved devices, will indeed reduce this burden. Shunts primarily fail due to obstruction of the shunt system with adherent inflammatory cells [33], [82], [91]–[94]. Astrocytes and macrophages are the dominant cell types bound directly to the catheter. Our recent work indicates that astrocytes make up more than 21% of cells bound to obstructed shunts. We have also observed that, of the obstructed masses blocking ventricular catheter holes, astrocytes makeup a vast

majority of cells. We have also found astrocyte markers in obstructive masses to be co-localized with proliferative markers, indicating that astrocytes are active on the shunt surface; they produce inflammatory cytokine IL-6 and proliferate [23], and their number and reactivity peak on failed shunts. In hydrocephalus patients, IL-6 cytokines significantly increase during shunt failure, especially after repeat failures. Astrocytes create a "glue" for further glia or other cells and tissues to secondarily bind and block the shunt. Even contact with the ventricular wall results in astrocyte migration to the surface and interaction with the shunt [95].

In this study, our goal is to reduce shunt obstruction by re-developing a strategy to reduce astrocyte activation and thus attachment and density on the shunt surface. Thus, we must control the degree of inflammatory cell activation. This is not the direct target of a specific treatment paradigm to date. We must first determine astrocyte phenotype expression in tissue that is obstructing shunts using failed patient's shunts, then employ a promising pharmacological agent that will inhibit the cell activation state to reduce attachment. The A1 reactive astrocytes are not as quickly proliferative, however, considerable proliferation of A2 reactive astrocytes is seen when the reactive response is to produce a protective scar around the injury [50]. Our goal is to observe whether the cells blocking shunts are expressing an A1 or A2 reactive astrocyte phenotype to understand how to diminish the cell immune response to shunts (Figure 4.1). That is to reduce mechanisms leading to shunt failure through inhibition of cell activation. To address this new research avenue, we use RNAscope fluorescent in situ hybridization and quantitative PCR analysis to determine the A1 or A2 reactive astrocyte phenotype expression on failed

shunt. ELISA analysis confirms the pro- and anti-inflammatory cytokine concentration profiles in the CSF associated with astrocyte activation. A powerful marker for A1 is the classical complement cascade component C3, specifically upregulated in A1 reactive astrocytes (and not in resting or A2 reactive astrocytes). C3 is one of the most characteristic and highly upregulated genes in A1 and EMP1 is an A2-specific gene. Then we employ the release of an FDA-approved pharmacological agent on the shunt surface that will inhibit the cell activation state to reduce the presence of astrocytes on shunts. This will keep any attaching astrocytes in a resting state, reduce proliferation, inhibit downstream proliferation, and ultimately deter shunt obstruction. Since the master cytokine IL-1 (α and β) is the initial molecular mediator that triggers glial scar formation around other devices in the brain, we will investigate whether astrocytes obstructing shunts could be prevented by simply blocking secretion or action of these cytokines to keep astrocytes out of the A1 or A2 reactive state. FDA-approved drugs targeting TNF-α, IL-1α and IL-1β already exist and are in use for other medical diseases.

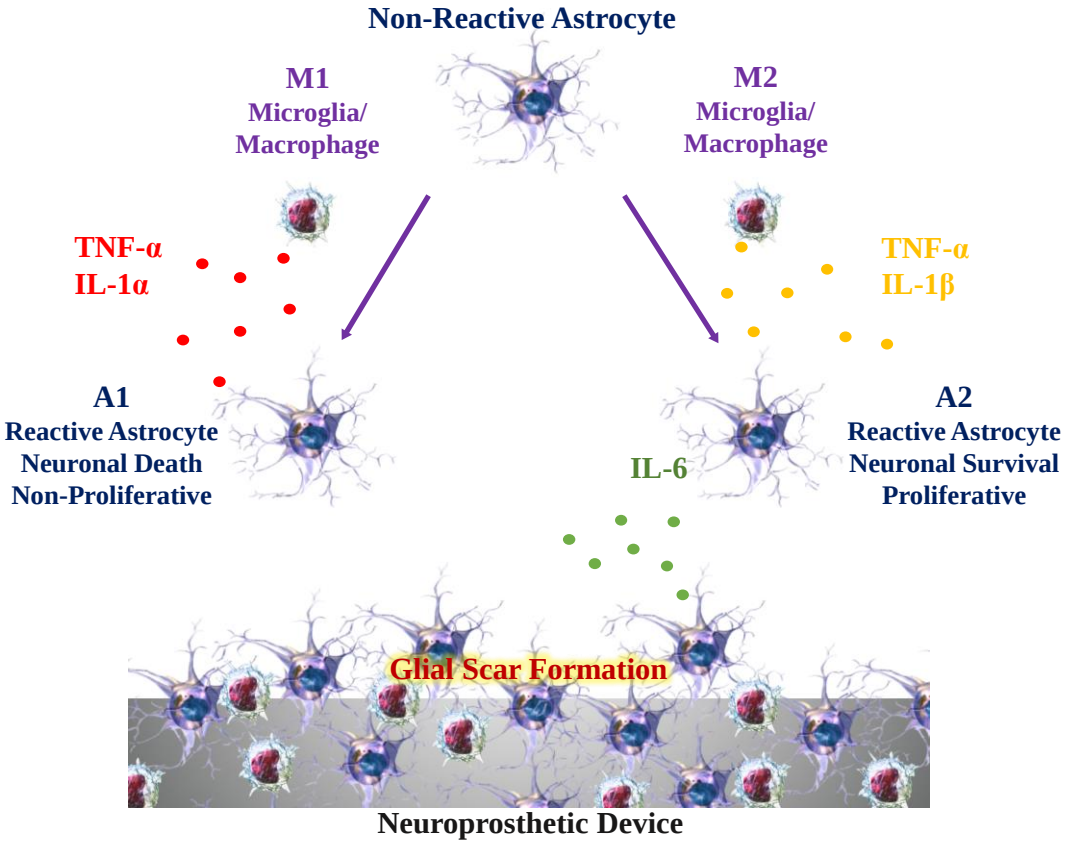

Figure 4.1. Microglia/macrophage and astrocyte reactions following neuroprothetic device implantation.
Injury changes microglia into an M1- and M2-like phenotype and astrocytes into an A1- and A2-type, respectively. Astrocytes and microglia work together to introduce either a neuroinflammatory or neuroprotective reaction after injury through the release of cytokines or neurotrophic factors that can lead to neuronal death or survival. The cytokine pathway is the best and most important measurable outcome for inflammatory cascades. Inflammatory cells at the brain-device interface communicate via cytokines to activate and recruit other inflammatory cells to the interface. Cytokine stimulation is a gateway for other gene products to be over- or under-expressed in the cascade, resulting in device failure. Therefore, the cytokine pathway is a starting point for mechanistic, thorough investigation of inflammation and device failure.

4.3. Materials and methods

4.3.1. Ethics approval

The permission to collect shunt hardware, CSF, and patient data was approved by the Wayne State Institutional Review Board (IRB) as the coordinating center and as a participating site. Written informed consent was obtained from all patients or their legally authorized representative. Collection was performed in a manner consistent with the standard of treatment; decision to remove the shunt was always based on clinical symptoms for surgical intervention chosen by the neurosurgeon. Samples were collected from individuals with any hydrocephalus etiology and clinical history. After removal by a surgeon, the shunt samples were immediately submerged in a solution of paraformaldehyde (PFA) to fix cells for RNAscope fluorescent in situ hybridization experiments or RNAlater, an aqueous, non-toxic tissue storage reagent that quickly saturates tissue to stabilize and protect the quality/quantity of cellular RNA in situ in unfrozen specimens for qPCR experiments. RNAlater removes the demand to instantly manage tissue specimens or to freeze samples in liquid nitrogen for later treatment. Obstructed and non-obstructed shunts were characterized based on the degree of actual tissue blockage on the shunt surface. A whole-mount procedure was used for all non-obstructed shunts, where the whole shunt was immersed in solution. For all obstructed shunts the tissue on the surface of the shunt was removed from the shunt. Tissue was then embedded in OCT compound for RNAscope fluorescent in situ hybridization experiments or immersed in solution for qPCR experiments. As previously described [96], CSF was collected at the time of shunt surgery and transported on ice to the Washington University Neonatal CSF Repository. Samples

were then centrifuged (2500 rpm for 6 min) at room temperature, and the supernatant was aliquoted and stored in 1.5 ml polypropylene microcentrifuge tubes at -80 °C until experimental analysis.

4.3.2. Quantitative PCR

Total RNA was extracted using the GenElute Mammalian Total RNA Miniprep Kit (sigma), cDNA synthesis was performed using the iScript cDNA Synthesis Kit (Bio-Rad), and qPCR was completed using the PowerUp SYBR Green Master Mix (Applied Biosystems) according to manufacturer protocols. Relative mRNA expression was normalized to hRPLP0 (reference gene) [97]. Primers for human are as follows: hC3 (A1 reactive astrocyte marker), hEMP1 (A2 reactive astrocyte marker) [98].

4.3.3. RNAscope fluorescent in situ hybridization

RNAscope fluorescent in situ hybridization was completed on fixed frozen tissue. Tissue was embedded in OCT compound (Tissue-Tek) and 14 μm tissue sections were prepared and immediately frozen at -80 °C. Multiplex RNAscope was performed according to manufacturer's (ACD: Advanced Cell Diagnostics) protocol against the target mRNA probes of hC3 (label for A1 reactive astrocytes), hEMP1 (label for A2 reactive astrocytes), and hSLC1A3 (label for astrocytes). RNAscope fluorescent in situ hybridization is nonlinearly amplified and hence intensity cannot be used to determine expression. Therefore, images were thresholded in ImageJ. The percent of area covered by this thresholded signal was then measured and verified as reactivity [97]. Images were acquired

with a resonance-scanning confocal microscopy (RS-G4 upright microscope, Caliber ID, Andover, MA, USA).

4.3.4. Multiplex ELISA

Multiplex assays were run by the Bursky Center for Human Immunology & Immunotherapy Programs (CHiiPs) at Washington University School of Medicine. Frozen supernatant CSF was slowly thawed and then analyzed in duplicate with multiplex immunoassay kits according to the manufacturer's instructions for the following inflammatory cytokines: IL-1α, IL-1β, IL-6, TNF-α, IL-8, IL-10 (Thermofisher Scientific), C3, and C1q (Millipore Sigma). Briefly, magnetic beads were added across all the wells on the plate, CSF samples and standards were then added in duplicate. Following washing steps, the detection antibody was added followed by streptavidin incubation. Beads were then resuspended with reading buffer and data were acquired on a Luminex detection system. The concentration of each analyte was calculated by plotting the expected concentration of the standards against the multiplex fluorescent immunoassay generated by each standard. A 4-parameter logistic regression was used for the best fit curve. Protein concentration is reported as pg/mL for each analyte.

4.3.5. Purification of astrocytes by immunopanning

Astrocytes were purified by immunopanning from post-natal day (P) 5 mouse brains and cultured as previously described [99]. Cerebral cortices were dissected and enzymatically digested using papain at 37 °C and 10% CO_2. Tissue was then mechanically

triturated with a serological pipette at RT to generate a single-cell suspension. The suspension was filtered and negatively panned for microglia/macrophage cells (CD45), oligodendrocyte progenitor cells (O4 hybridoma), and endothelial cells (L1) followed by positive panning for astrocyte cells (ITGB5). Astrocytes were cultured in defined, serum-free medium containing 50% neurobasal, 50% DMEM, 100 U/mL penicillin, 100 μg/mL streptomycin, 1mM sodium pyruvate, 292 μg/mL L-glutamine, 1× SATO, 5 μg/mL of N-acetyl cysteine, and 5 ng/mL HBEGF.

All animal protocols were approved by the Institutional Animal Care and Use Committee at Wayne State University (IACUC).

4.3.6. Targeted drug delivery

A1 reactive astrocytes were generated by culturing the purified astrocytes on PDMS coated tissue culture plates and then treating for 24 h with IL-1α (3 ng/ml, Sigma, I3901), TNF-α (30 ng/ml, Cell Signaling Technology, 8902SF), and C1q (400 ng/ml, MyBioSource, MBS143105). A2 reactive astrocytes were generated by culturing the purified astrocytes on PDMS coated tissue culture plates and then treating for 24 h with IL-1β (30 ng/ml, Cell Signaling Technology, 8900SF) and TNF-α (30 ng/ml, Cell Signaling Technology, 8902SF). A1 reactive astrocytes were targeted for 48 h using neutralizing antibodies to IL-1α (30 ng/ml, Abcam, ab9614), TNF-α (30 ng/ml, Cell Signaling Technology, 7321), and TGF-β (30 ng/ml, R&D Systems, 243-B3-002/CF). A2 reactive astrocytes were targeted for 48 h using neutralizing antibodies to IL-1β (30 ng/ml,

Abcam, ab9722), TNF-α (30 ng/ml, Cell Signaling Technology, 7321), and IL-6 (30 ng/ml, Abcam, ab6672) [70], [100].

Polydimethylsiloxane (PDMS) coated tissue culture plates were prepared by mixing Sylgard-184 elastomer and curing agents at a ratio of 10:1 (w/v), then pouring into the plates and curing for 48 h.

4.3.7. Data presentation and statistical analysis

All data presented was performed using GraphPad Prism version 8. Two-tailed unpaired Student's t-test and two-way ANOVA test was performed. The mean with standard error mean (for the experiments done independently with technical replicates) and standard deviation was displayed. A predetermined significance level of $P < 0.05$ was used in all statistical tests.

4.4. Results and discussion

4.4.1. The inflammatory response following shunt implantation

Quantitative PCR (qPCR) was performed on collected tissue from failed shunts received from patients. Since the tissue obstructing shunts comprises of a more exaggerated astrocytic response, we investigated the up-regulation of the A1-specific reactive gene C3 and the A2-specific reactive gene EMP1. We observed that a heterogeneous up-regulation of both the A1- and the A2-specific reactive gene exist on both obstructed and non-obstructed shunts with no significant difference. In addition, we observed an increase in

the EMP1 expression on non-obstructed shunts, while an increase in the C3 expression was noticed on obstructed shunts (Figure 4.2).

Indeed, A1 reactive astrocytes are a major source of the classical complement cascade component C3, however, other inflammatory cells in the tissue on obstructed shunts also induce the expression of C3. The increased expression of C3 on obstructed shunts is in accordance with other studies linking persistent neuroinflammation to neurodegeneration and adverse effects on the neural circuits and decrease excitatory neuronal function [101]. This is to recruit additional immunocytes to the site and exacerbate the secondary insult response.

Astrocytes are the dominant cell type bound directly to non-obstructed shunts and play a neuroprotective role, particularly in the acute phase of injury following an immediate disruption of the blood-brain barrier (BBB). Therefore, the increased expression of EMP1 on non-obstructed shunts is in accordance with other studies [94].

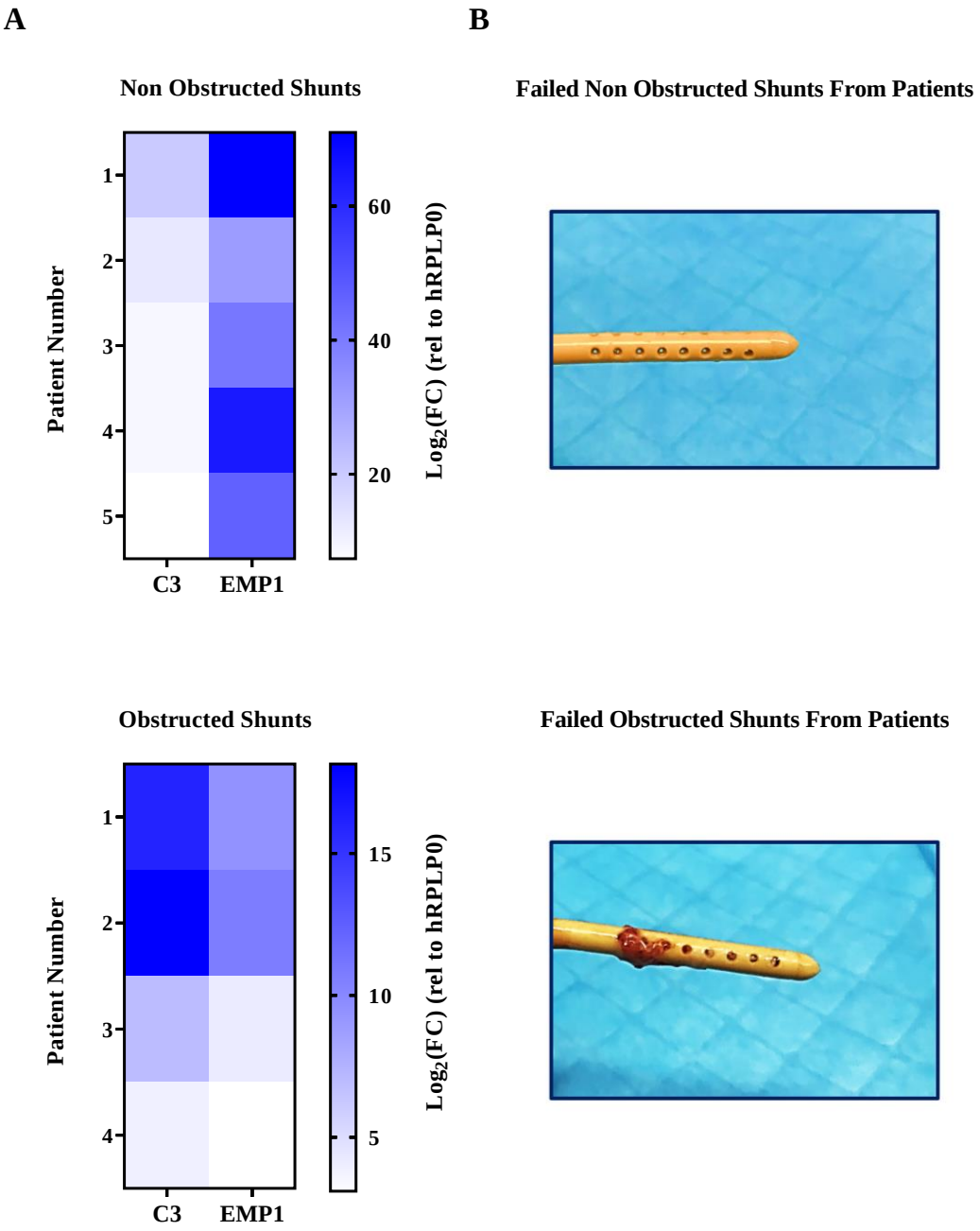

Figure 4.2. Expression of C3, EMP1 astrocyte activation genes assessed by qPCR on obstructed and non-obstructed shunts.
(A) Heat map comparing the expression of A1-specific reactive gene C3 and the A2-specific reactive gene EMP1 for obstructed and non-obstructed shunts collected from patients (two-way ANOVA test). (B) Representative images for obstructed and non-obstructed shunts.

4.4.2. The astrocyte phenotype expression on implanted shunts

RNAscope fluorescent in situ hybridization was performed on collected tissue from failed shunts received from patients. In accordance with our qPCR data, we found that the majority of SLC1A3+ astrocytes express A1 (C3) and/or A2 (Emp1) markers, suggesting that astrocytes can express a combination of A1 and A2 genes on shunt surfaces. In particular, we observed that a greater number of SLC1A3+ astrocytes expressed the A2-specific gene Emp1 on both obstructed and non-obstructed shunts. Interestingly, the number of A2 reactive astrocytes are significantly larger on obstructed shunts compared to A1 reactive astrocytes (Figure 4.3). In our recent work, we have also observed astrocyte markers in obstructive masses to be co-localized with proliferative markers, indicating that astrocytes are active on the shunt surface: they produce inflammatory cytokine IL-6 and proliferate. Since A2 reactive astrocytes are proliferative [50], they are responsible for the glial scar formation observed on obstructed shunts. This is in accordance with other studies, indicating that glial scar borders are formed by newly proliferated astrocytes that recruit inflammatory and fibrotic cells via STAT3-dependent methods [72], and that astrocytes in scar formation seem to be devoid of C3 upregulation [102].

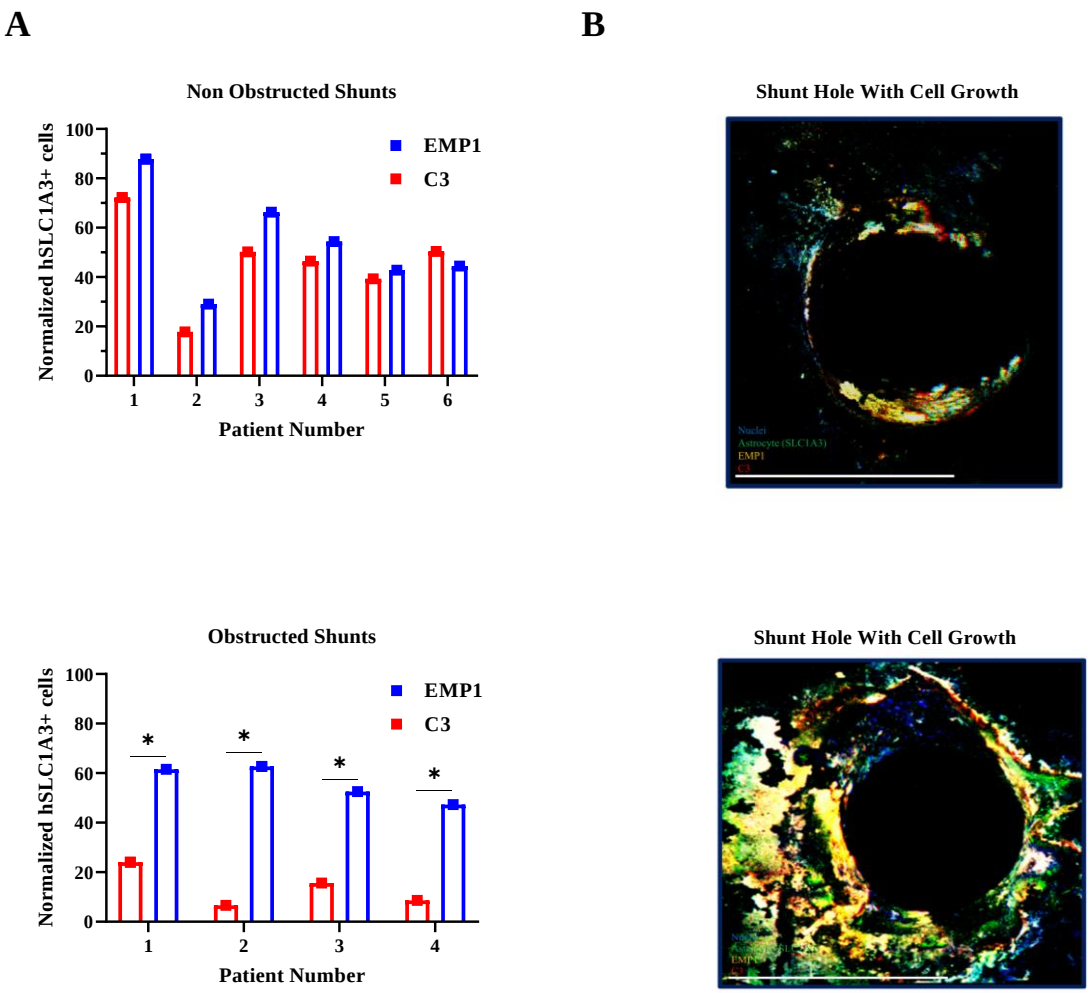

Figure 4.3. Comparison of astrocyte response by RNAscope fluorescent in situ hybridization on obstructed and non-obstructed shunts.
(A) The astrocyte phenotype specificity of C3 and EMP1 RNAscope fluorescent in situ hybridization signal was assessed by probing for SLC1A3+ astrocytes on both obstructed and non-obstructed shunts collected from patients. For normalization, the C3 and EMP1 signals were dividing by SLC1A3 signals (*$p < 0.05$; two-way ANOVA test). (B) Representative RNAscope fluorescent in situ hybridization images for obstructed and non-obstructed astrocyte gene C3 (red) and EMP1(yellow) showing colocalization with the astrocyte marker SLC1A3 (green) (scale bar = 500 μm).

4.4.3. CSF biomarkers in obstructed and non-obstructed shunts

Using multiplex ELISA, this study investigated shunt failure through the CSF protein concentration profiles of select pro-inflammatory and anti-inflammatory cytokines for obstructed and non-obstructed shunts. C1q, IL-1α, and TNF-α induce A1 reactive astrocytes, IL-1β, TNF-α and IL-6 induce A2 reactive astrocytes. C3 is an A1 astrocyte marker. IL-8 and IL-10 inflammatory cytokines are of interest as they consistently stand out by being elevated in the CSF of hydrocephalus patients. Remarkably, in accordance with our qPCR data, we found higher neuroinflammation for obstructed shunts, however, with no significant difference compared to non-obstructed shunts confirming the heterogeneous mixed population of both the A1 and the A2 reactive astrocytes. Interestingly, higher levels of IL-6 are observed for obstructed shunts compared to non-obstructed shunts (Figure 4.4). As indicated in the RNAscope fluorescent in situ hybridization results, IL-6 primarily activates A2 reactive astrocyte proliferation through a positive feed-forward loop, activating local astrocytes to maintain the glial scar formation on the shunt surface.

In our recent paper, higher levels of IL-6 are observed for non-obstructed shunts compared to obstructed shunts [96]. However, obstructed and non-obstructed shunts were characterized based on the symptoms of obstruction defined by the patient's charts instead of the degree of actual tissue blockage on the shunt surface as described in this study.

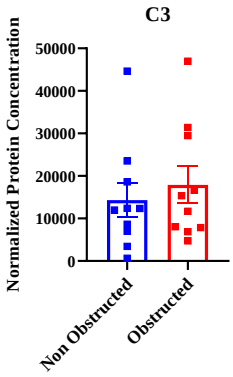
C3
Normalized Protein Concentration
50000
40000
30000
20000
10000
0
Non Obstructed
Obstructed

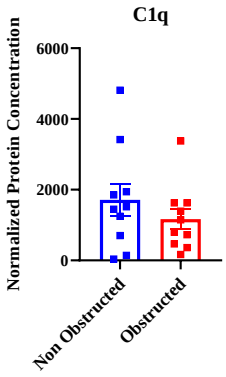
C1q
Normalized Protein Concentration
6000
4000
2000
0
Non Obstructed
Obstructed

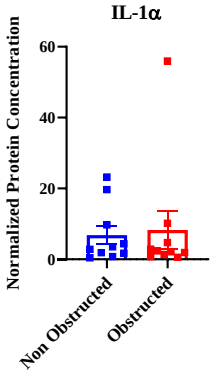
IL-1α
Normalized Protein Concentration
60
40
20
0
Non Obstructed
Obstructed

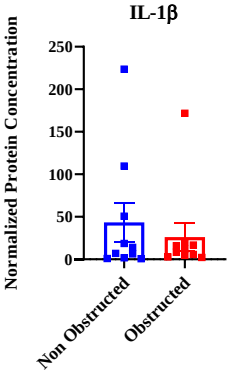
IL-1β
Normalized Protein Concentration
250
200
150
100
50
0
Non Obstructed
Obstructed

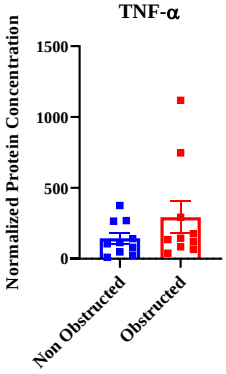
TNF-α
Normalized Protein Concentration
1500
1000
500
0
Non Obstructed
Obstructed

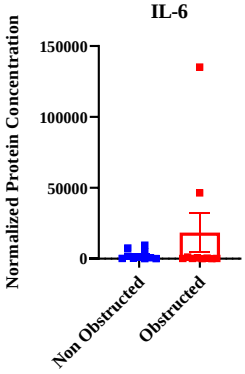
IL-6
Normalized Protein Concentration
150000
100000
50000
0
Non Obstructed
Obstructed

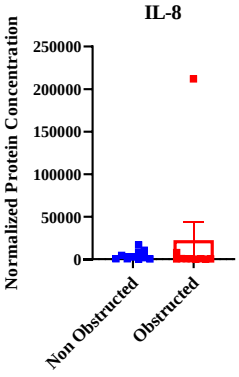
IL-8
Normalized Protein Concentration
250000
200000
150000
100000
50000
0
Non Obstructed
Obstructed

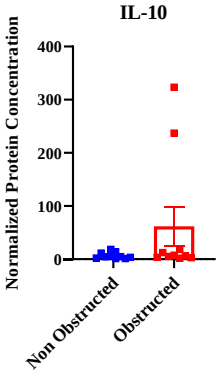
IL-10
Normalized Protein Concentration
400
300
200
100
0
Non Obstructed
Obstructed

Figure 4.4. Cerebrospinal fluid cytokine concentrations between obstructed and non-obstructed shunts.
Analytes include C3, C1q, and IL-1α (A1 astrocyte markers), IL-1β and IL-6 (A2 astrocyte markers), TNF-α, IL-8 and IL-10. For normalization, the concentration of each cytokine is divided by the total protein concentration for each group (two-tailed unpaired Student's t-test, n = 10 per group, mean ± SEM).

4.4.4. Inhibiting astrocyte cell activation

Now we understand that a heterogeneous mixed population of both the A1 and A2 reactive phenotype exist on the shunt surface. In addition, TNFα, IL-1α combined propel resting astrocytes into an A1 reactive phenotype [70] and co-stimulation with TNF-α and IL-1β induces an A2 reactive astrocyte phenotype [49]. Also, IL-6 induces astrogliosis and astrocyte proliferation [23]. Therefore, we investigated whether the activity of astrocytes could be significantly reduced by simply employing already FDA-approved antibody therapies that inhibit human TNF-α, IL-1α, IL-1β, and IL-6. Hence, neutralizing antibodies to TNF-α, IL-1α, IL-1β and IL-6 were employed to decrease the activity of A1 and A2 astrocytes for a significant decrease in attachment on PDMS coated surfaces mimicking the shunt surface (Figure 4.5). These data are in accordance with other studies indicating that the knockout of reactive astrocyte activating factors slows disease progression [97], dampening the formation of reactive astrocytes prevents neuronal death [100], and astrogliosis inhibition attenuates hydrocephalus [103].

The anti-inflammatory cytokine TGF-ß was able to reset A1 astrocytes to a non-reactive state, significantly reducing cell attachment on the PDMS coated surface. This is in accordance with other studies indicating that TGF-ß suppresses A1 astrocyte activation [70], reverses the formation of A1 astrocytes by fibroblast growth factor (FGF) signaling

[104], and greatly reduces the expression of A1-specific markers [105]. Furthermore, TGF-β did not induce A2 reactive astrocyte attachment on the PDMS coated surface.

Taken together, these data suggest that drug therapies could eventually be added to the shunt as device coating and released in vivo for enhanced next-generation medical devices.

A

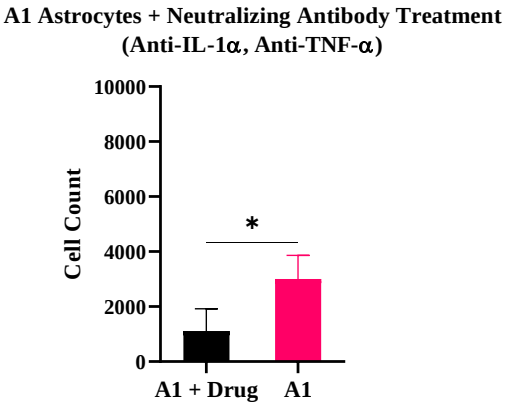

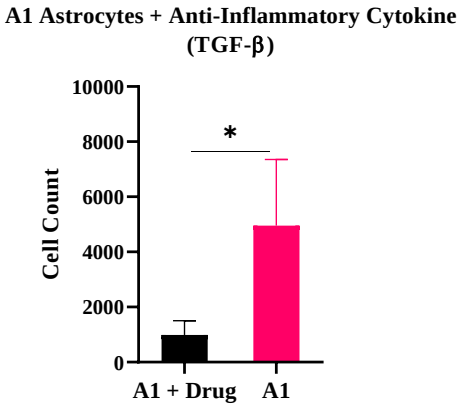

B

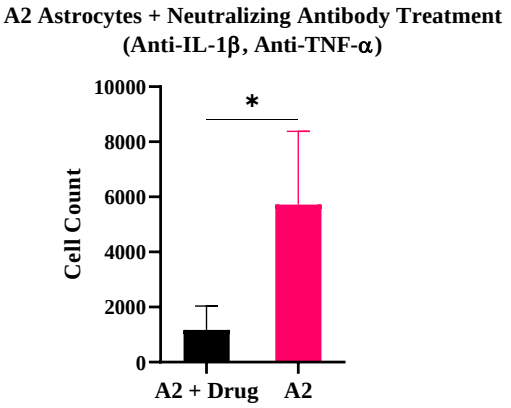

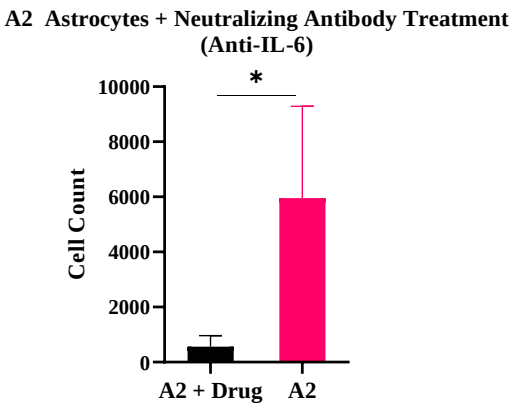

Figure 4.5. Antibody therapies that will inhibit the cell activation state to reduce attachment on the shunt surface.
(A) A1 reactive astrocytes treated with neutralizing antibodies to TNF-α, IL-1α, and anti-inflammatory cytokine TGF-β. (B) A2 reactive astrocytes treated with neutralizing antibodies to TNF-α, IL-1β, and IL-6 (*$p < 0.05$; two-tailed unpaired Student's t-test, n = 3 per group, mean ± SD).

4.5. Directions for future applications

This first-time study, which pulls strengths from the recent world-renowned Barres et al. study on astrocyte activation, represents a robust investigation of the changes in gene expression levels specific to astrocyte immune response following CSF shunt implantation. By shedding light on the mystery of astrocyte phenotype expression on shunt surfaces, root causes for shunt failure can be achieved to improve hydrocephalus treatment.

Cell adhesion is not necessary to drive the neuroinflammatory response and biomaterials that go beyond reducing cell adhesion alone but also incorporate improved attenuation of inflammation in the tissue surrounding the implanted device are required. In extensive studies, chronically implanted neural implants with coatings were compared to that of identical uncoated devices. In vitro, the coated implant significantly reduced astrocyte and microglial adhesion by ~95%. A similar reduction of cell adhesion was observed following device removal after two, four or 24 weeks of implantation in rat cortical tissue. Interestingly, no significant difference was observed in the neuro-inflammatory response or the level of neuronal loss surrounding the coated implant compared to uncoated devices. A persistent inflammation was observed surrounding both uncoated and coated implants. Furthermore, neuronal density around the implanted devices was also lower for both implant groups compared to the uninjured controls. As no cells

were found adhered to coated implants upon removal, both coatings were still functioning at the endpoints studied.

Our recent paper also indicates that under higher shear stress, despite less cell attachment to the surface, a significant increase in IL-6 secretion is detected [23]. Our data support others, which recognize a requirement for the control of the degree of inflammatory cell activation for significant improvement of device function within the brain, in contrast to the general in vivo implant failure only based on decreased cell adhesion on the device surface [26], [58]–[60]. Our results are in arrangement with other studies and present a proof of concept that to have significant effect, approaches should emphasis on reducing the initial inflammatory cell activation instead of only targeting cell adhesion reduction on the device surface. Such approaches involve decreasing shear activation as a primary cause of device failure [10], [14], [26], [27], [34]–[36], [86], and directly reducing the buildup of inflammatory cytokines through targeted therapeutic for TNF-α, IL-1α, Il-1β, and IL-6.

The complications for targeted drug delivery to A1 and A2 reactive astrocytes will be establishing the parameters for delivery and the delivery vehicle for device coating in vivo. Cytokine responses were highly upregulated within a day post implantation, suggesting that cytokine targeting approaches need to be present at the site of implantation immediately following implantation. However, many inflammatory cytokine targeting agents act like double-edged swords. Given that the targeting agents are concentration dependent, the goal must be to suppress any unnecessary activation rather than to eliminate all activity.

4.5.1. Capturing and neutralizing inflammatory cytokines

Some therapeutic agents bind with cytokines for neutralization directly, whereas others bind with cognate receptors on the target cell surface to block their interaction with incoming cytokines. Also, some agents induce the internalization or downregulation of cytokine receptors of the target cells, thereby, restricting cytokine-triggered cell activation. Furthermore, compounds that induce clearance of the target cells are also used to reduce the overall cytokine response. In general, anti-cytokine agents that directly capture and neutralize cytokines could avoid interactions with cytokine receptors on the target cells, and thus, are less likely to be internalized and cleared by the target cells. Moreover, capturing and neutralizing free cytokines instead of targeting cell receptors also reduces the transmission of intracellular signals, which might stimulate adverse events such as immune system impairment [106]. Monoplex platforms such as cytokine-neutralizing antibodies and antibodies conjugated with biomaterials are designed with one specific cytokine as the target. Multiplex platforms such as cell-membrane-coated nanoparticles are designed for simultaneously neutralizing multiple cytokines involved in inflammatory diseases.

4.5.1.1. Biomaterial-conjugated antibodies

One limiting factor of free antibodies is their dose-limiting side effects related to the nonselective biodistribution. To resolve this limitation, antibodies have been conjugated with biomaterials to alter their in vivo pharmacokinetics for a favorable therapeutic biodistribution. Furthermore, the biomaterial conjugation could also expand the

use of antibodies to areas where free antibodies were unable to access. These advantages have led to cytokine-neutralizing antibodies conjugated with various biomaterial platforms, including polymers, hydrogels, and nanoparticles for a wide range of biomedical applications.

4.5.1.1.1. Polymer-antibody conjugate

Conjugation with polymers could increase the molecular weight of the antibodies and limit their diffusion rate and significantly increase the antibody residence time when administered to tissues, making the conjugates ideal for localized inflammatory treatment via fewer immune cells infiltration such as inhibition of macrophage activation. Measurements of local antibody concentration showed that the increased antibody residence time in the superficial region strongly correlated with the pattern of inflammatory cell infiltrate in the tissue. Notably, in polymer-antibody conjugates, the polymer backbone could affect the antibody-cytokine binding affinity depending on the use of polymers for a slower dissociation. In addition to the polymer backbone, the size of cytokine targets would also affect the binding kinetics which might become a key factor in binding events and outperform the effect from the polymer backbone.

4.5.1.1.2. Hydrogel-antibody conjugate

Conjugation of cytokine-neutralizing antibodies with hydrogels is another method of modifying local inflammation while minimizing the systemic side effects associated with free antibodies. However, the high density of the hydrogel cross-linking, limited

cytokine diffusion into the gel matrix and reduced the neutralization efficiency. Therefore, hydrogel cross-linking density needs to be optimized to maintain gel-like properties while maximizing cytokine influx for effective neutralization. Meanwhile, tuning the residence time of cytokine-neutralizing antibodies could be an effective approach in controlling the inflammatory response associated with acute injuries. Microelectrodes have been engineered to encapsulate and release scar-inhibiting agents [107].

4.5.1.1.3. Nanoparticle-antibody conjugate

Cytokine-neutralizing antibodies are conjugated with nanoparticles for advantages, including enhanced stability, specific targeting, and prolonged retention after local injection. Also, antibody immobilization on the nanoparticles reduced their degradation. For example, in a study concerning the treatment of acute temporal lobe epilepsy (TLE) in an acute rat model, superparamagnetic iron-oxide nanoparticles were coated with PEG and then conjugated with an anti-IL-1β antibody. The resulting nanoparticle–antibody conjugates not only improved the neuroprotective effect in the acute TLE rat model through IL-1β neutralization but also targeted the magnetic nanoparticles to the astrocytes and neurons in the epileptogenic tissues, leading to a higher contrast in magnetic resonance imaging (MRI) than the nanoparticles without antibody conjugation [108]. Nanoparticles as smart approaches offer opportunities for accurately delivering drugs in dose-, spatial- and temporal-controlled methods (Table 2).

Table 2. Key advantages and disadvantages of major anti-cytokine platforms.

Major Anti-cytokine Platforms	Pros	Cons
Free antibody	- Well-established drug development pathways	- Limited local retention
Biomaterial conjugated antibody	- Local administration - Tunable pharmacokinetics through controlled biomaterial degradation	- Requires covalent conjugation with possibility of denaturing the protein
Hydrogel conjugated antibody	- Widely available and low cost	- Cytokine binding profiles are poorly defined
Nanoparticle conjugated antibody	- Versatile coating materials for various substrates	- Need to verify immune compatibility

4.5.1.1.4. Exosomes

Exosomes are nanoparticles produced by almost all cells and they facilitate cell-cell communication by transporting biomolecules and circulating them in body fluids, and all cells can take them up. Thus, amenable to every therapeutic area for diagnostic markers and therapeutic delivery vehicles. They safely and efficiently transfer their cargo biomaterials between source and recipient cells over long distances with low immunogenicity. Exosomes are increasingly employed as therapeutic vehicles to enhance CNS diseases and damage such as stroke and traumatic brain injury through enriched beneficial cargos for example microRNA (miRNA) [109]. Compared with cell-based therapy, exosomes are easily harvested and generated at large-scale from cells. Exosomes

can cross the blood-brain barrier (BBB) and directly target cells, increase M1/M2 polarization, reduce neuroinflammation, inhibit Toll-like receptor (TLR) and NF-κB signaling pathway. When injected into the bloodstream, they reach the brain, switched off the gene and even reduce levels of protein.

Synthetic nanoparticle delivery devices have mainly been employed for RNA therapies. However, they produce toxic immune reactions in humans and are discreditable for accumulation in the liver. Exosomes are without any obvious immune reactions and most of them are delivered [110].

4.5.2. Gradual drug release

Studies that delivered drugs locally around an implanted device, displayed reactivity of cells at later time points due to drug being consumed at the initial phase. Therefore, a more long-lasting drug delivery will be required to control the neuroinflammatory response through the lifetime of the implanted device. An implant injury leads to a chronic foreign body response that is well-characterized and shown to affect the device−tissue interface stability. Several strategies have been applied to modulate the immune response, including the application of immunomodulatory drugs applied both systemically and locally. While the use of passive drug release at the site of injury has been exploited to minimize neuroinflammation, this strategy has all but failed as the anti-inflammatory drugs are released at predetermined times that are often inconsistent with the ongoing innate inflammatory process. Engineering a sustained release of the anti-

inflammatory drug over extended periods of time, paves the way to fabricate neuroprosthetic devices capable of attenuating the foreign body response [111]–[114].

4.5.2.1. Sequential release

To achieve sequential release profile, a drug is physically adsorbed onto the hydrogels for fast release, while the second drug is attached via for example biotin and streptavidin binding for sustained release. Exploiting biotin-streptavidin interactions affords control over the release of drugs without drastically altering the bio-functionality of the hydrogels, which might occur with other controlled release systems such as coatings. Thus, the hydrogel system enables timing sequential release of different drugs [115].

4.5.2.2. Composite surfaces

Short-term delivery of anti-cytokine therapies are incapable of providing constant therapeutic benefits due to low bioavailability and fast clearance rates. To develop a system to provide constant protection, initial burst release followed by constant demonstration of an immobilized layer of the neutralizing antibody must be utilized [116]. For an unmodified electrode, microglia/macrophages cells adhere to the surface of the device and release high amounts of inflammatory species. the presence of composite surfaces results in decrease in localized inflammation from activated microglia/macrophages.

Neuroinflammation is organized by a variety of cytokines; therefore, neutralization of one or a few cytokines is inadequate to stop or reverse disease progression. Also, cytokines are immediately released during the first few minutes after injury, triggering

rapid cellular infiltration and fast development of neuroinflammation. Thus, alternative anti-inflammatory methods that rapidly regulate a variety of inflammatory cytokines are highly advantageous to inhibit neuroinflammation-induced injury and promote functional recovery. Furthermore, to achieve simultaneously capturing the released cytokines and inhibiting the synthesis of new ones in a broad-spectrum manner a core/shell-structured microcomposite design efficiently neutralizes the excessive cytokines immediately after injury. Meanwhile, the controlled release of immunosuppressive drug reduces the secretion of new inflammatory cytokines. Therefore, the core/shell-structured microcomposite restrains the recruitment of macrophages leading to an improved recovery [117].

4.5.2.3. layer-by-layer technique

Modes of delivery that release only the desired amount of drug over the appropriate time frame and must be delivered in combination, for example, the administration of both an anti-inflammatory and an antibiotic drug, there is usually a different desired rate and amount of release for each compound, depending on the function of the therapeutic and its half-life in the body. Layer-by-layer (LbL) controlled release combines therapeutics directly into thin films with varying adsorptions based on charge, hydrogen bonding, or other interactions and releases the drug in a sequential manner [118]. The ability of creating thin films from water directly, without the requirement for additional chemical modifications of the film components, allows the direct incorporation of growth factors, DNA, antibodies, and other biologic drugs via electrostatic or hydrogen bonds. The films can undergo degradation or release by the incorporation of hydrolytically or enzymatically

degradable polymers. The capability to achieve high loadings while enabling very controlled release patterns in the delivery of both small-molecule and biologic drugs with limited range of release behaviors is an advantage of LbL techniques. By placing drug containing layers in the film in a systematic pattern, LbL film architectures that each have their own relative rates of release and unique release profiles are designed. A film can be assembled from the bottom up to create controlled corelease or sequential release patterns that are consistent with the desired therapeutic treatment. For singular drugs, LbL approach supports stable, uniform coatings that can release in long or short profiles or with a combination of release profiles, for example, a burst release followed by sustained release profile. For the release of two or more drugs, LbL coatings incorporates dissimilar drugs into one uniform thin film and independently controls the release of each therapeutic. The management of these release profiles can lead to much more synergistic drug-release profiles informed by native biological processes [119], [120].

4.6. Conclusion

First-time revealing of astrocyte phenotype expression leads to (1) a precise understanding of cellular response mechanism to device implantation and a precise interpretation of failure in chronically indwelling neuroprosthetics, (2) a therapeutic window for more targeted therapies to inhibit astrocyte activation and attachment on the implant. Therefore, for significant reduction in device failure, alongside manipulating shunt properties, drug therapy is used for inhibition of cytokines and therefore inhibition of cell aggregation for achieving stable and long-term functional outcomes. A complete

approach that is based on improved understanding of underlying biological processes, is intelligently designed, and therefore will increase advancements in hydrocephalus shunt technology that will one day be utilized for real clinical applications.

REFERENCES

[1] A. Campbell and C. Wu, “Chronically implanted intracranial electrodes: Tissue reaction and electrical changes,” *Micromachines*, vol. 9, no. 9, pp. 1–14, 2018.

[2] Y. Zhong and R. V Bellamkonda, “Biomaterials for the central nervous system.,” *J. R. Soc. Interface*, vol. 5, no. 26, pp. 957–75, Sep. 2008.

[3] T. D. Y. Kozai, A. S. Jaquins-Gerstl, A. L. Vazquez, A. C. Michael, and X. T. Cui, “Brain tissue responses to neural implants impact signal sensitivity and intervention strategies,” *ACS Chem. Neurosci.*, vol. 6, no. 1, pp. 48–67, 2015.

[4] J. Lin, M. Morris, W. Olivero, F. Boop, and R. A. Sanford, “Computational and experimental study of proximal flow in ventricular catheters: Technical note,” *J. Neurosurg.*, vol. 99, no. 2, pp. 426–431, 2003.

[5] M. Galarza, Á. Giménez, O. Pellicer, J. Valero, and J. M. Amigó, “New designs of ventricular catheters for hydrocephalus by 3-D computational fluid dynamics,” *Child’s Nerv. Syst.*, vol. 31, no. 1, pp. 37–48, 2015.

[6] S. H. Weisenberg, S. C. TerMaath, C. N. Barbier, J. C. Hill, and J. A. Killeffer, “A computational fluid dynamics simulation framework for ventricular catheter design optimization,” *J. Neurosurg.*, vol. 129, no. 4, pp. 1067–1077, 2018.

[7] Y. K. Kim, E. Y. Chen, and W. F. Liu, “Biomolecular strategies to modulate the macrophage response to implanted materials,” *J. Mater. Chem. B*, vol. 4, no. 9, pp. 1600–1609, 2016.

[8] M. D. Swartzlander, C. A. Barnes, A. K. Blakney, J. L. Kaar, T. R. Kyriakides, and S. J. Bryant, “Linking the foreign body response and protein adsorption to

PEG-based hydrogels using proteomics," *Biomaterials*, vol. 41, pp. 26–36, 2015.

[9] H. W. Bedell, N. J. Schaub, J. R. Capadona, and E. S. Ereifej, "Differential expression of genes involved in the acute innate immune response to intracortical microelectrodes," *Acta Biomater.*, vol. 102, pp. 205–219, 2020.

[10] J. K. Hermann *et al.*, "The role of toll-like receptor 2 and 4 innate immunity pathways in intracortical microelectrode-induced neuroinflammation," *Front. Bioeng. Biotechnol.*, vol. 6, no. AUG, pp. 1–17, 2018.

[11] L. Tarassishin, H. S. Suh, and S. C. Lee, "LPS and IL-1 differentially activate mouse and human astrocytes: Role of CD14," *Glia*, vol. 62, no. 6, pp. 999–1013, 2014.

[12] L. Karumbaiah *et al.*, "Relationship between intracortical electrode design and chronic recording function," *Biomaterials*, vol. 34, no. 33, pp. 8061–8074, 2013.

[13] Y. Shinozaki *et al.*, "Transformation of Astrocytes to a Neuroprotective Phenotype by Microglia via P2Y1 Receptor Downregulation," *Cell Rep.*, vol. 19, no. 6, pp. 1151–1164, 2017.

[14] W. He and R.V. Bellamkonda, "A molecular perspective on understanding and modulating the performance of chronic central nervous system (CNS) recording electrodes," *Chapter 6Publisher CRC Press. William M Reichert*, 2008.

[15] M. V Sofroniew, "Astrogliosis," *Cold Spring Harb. Perspect. Biol.*, vol. 7, no. 2, pp. 1–16, 2015.

[16] P. Hariharan and C. A. Harris, *Shunts and Shunt Malfunction*. 2019.

[17] M. V. Sofroniew, "Astrocyte Reactivity: Subtypes, States, and Functions in CNS

Innate Immunity," *Trends Immunol.*, vol. 41, no. 9, pp. 758–770, 2020.

[18] M. V. Sofroniew, "Astrocyte barriers to neurotoxic inflammation," *Nat. Rev. Neurosci.*, vol. 16, no. 5, pp. 249–263, 2015.

[19] P. Moshayedi *et al.*, "The relationship between glial cell mechanosensitivity and foreign body reactions in the central nervous system," *Biomaterials*, vol. 35, no. 13, pp. 3919–3925, 2014.

[20] T. W. Hsiao, V. P. Swarup, B. Kuberan, P. A. Tresco, and V. Hlady, "Astrocytes specifically remove surface-adsorbed fibrinogen and locally express chondroitin sulfate proteoglycans," *Acta Biomater.*, vol. 9, no. 7, pp. 7200–7208, 2013.

[21] W. G. Brodbeck, Y. Nakayama, T. Matsuda, E. Colton, N. P. Ziats, and J. M. Anderson, "Biomaterial surface chemistry dictates adherent monocyte/macrophage cytokine expression in vitro," *Cytokine*, vol. 18, no. 6, pp. 311–319, 2002.

[22] N. F. Nolta, M. B. Christensen, P. D. Crane, J. L. Skousen, and P. A. Tresco, "BBB leakage, astrogliosis, and tissue loss correlate with silicon microelectrode array recording performance," *Biomaterials*, vol. 53, pp. 753–762, 2015.

[23] F. Khodadadei, A. P. Liu, and C. A. Harris, "A high-resolution real-time quantification of astrocyte cytokine secretion under shear stress for investigating hydrocephalus shunt failure," *Commun. Biol.*, vol. 4, no. 1, pp. 1–10, 2021.

[24] J. R. Eles *et al.*, "Neuroadhesive L1 coating attenuates acute microglial attachment to neural electrodes as revealed by live two-photon microscopy," *Biomaterials*, vol. 113, pp. 279–292, 2017.

[25] M. Ravikumar *et al.*, "The roles of blood-derived macrophages and resident

microglia in the neuroinflammatory response to implanted Intracortical microelectrodes," *Biomaterials*, vol. 35, no. 28, pp. 8049–8064, 2014.

[26] M. Jorfi, J. L. Skousen, C. Weder, and J. R. Capadona, "Progress towards biocompatible intracortical microelectrodes for neural interfacing applications," *Journal of Neural Engineering*, vol. 12, no. 1. IOP Publishing, p. 11001, 2015.

[27] K. C. Spencer, J. C. Sy, K. B. Ramadi, A. M. Graybiel, R. Langer, and M. J. Cima, "Characterization of Mechanically Matched Hydrogel Coatings to Improve the Biocompatibility of Neural Implants," *Sci. Rep.*, vol. 7, no. 1, pp. 1–16, 2017.

[28] J. P. Harris *et al.*, "Mechanically adaptive intracortical implants improve the proximity of neuronal cell bodies," *J. Neural Eng.*, vol. 8, no. 6, 2011.

[29] J. K. Nguyen *et al.*, "Mechanically-compliant intracortical implants reduce the neuroinflammatory response," *J. Neural Eng.*, vol. 11, no. 5, 2014.

[30] S. B. Michael Polanco, Hargsoon Yoon, "Micromotion-induced dynamic effects from a neural probe and brain tissue interface," *J. Micro/Nanolithography, MEMS, MOEMS*, vol. 13, 2014.

[31] E. S. Ereifej *et al.*, "Nanopatterning effects on astrocyte reactivity," *J. Biomed. Mater. Res. - Part A*, vol. 101 A, no. 6, pp. 1743–1757, 2013.

[32] Giménez, M. Galarza, U. Thomale, M. U. Schuhmann, J. Valero, and J. M. Amigó, "Pulsatile flow in ventricular catheters for hydrocephalus," *Philos. Trans. R. Soc. A Math. Phys. Eng. Sci.*, vol. 375, no. 2096, 2017.

[33] C. Harris *et al.*, "Fabrication of three-dimensional hydrogel scaffolds for modeling shunt failure by tissue obstruction in hydrocephalus," *Fluids Barriers CNS*, vol.

12, no. 1, pp. 1–15, 2015.

[34] C. A. Harris and J. P. McAllister, “Does drainage hole size influence adhesion on ventricular catheters?,” *Child’s Nerv. Syst.*, vol. 27, no. 8, pp. 1221–1232, 2011.

[35] C. A. Harris, J. H. Resau, E. A. Hudson, R. A. West, C. Moon, and J. P. McAllister, “Mechanical contributions to astrocyte adhesion using a novel in vitro model of catheter obstruction,” *Exp. Neurol.*, vol. 222, no. 2, pp. 204–210, 2010.

[36] C. A. Harris *et al.*, “Effects of surface wettability, flow and protein concentration on macrohage and astrocyte adhesion in an in vitro model of central nervous system catheter obstruction,” *J. Biomed. Mater. Res. Part A*, vol. 97, no. 4, pp. 433–440, 2011.

[37] J. C. Love, J. L. Ronan, G. M. Grotenbreg, A. G. Van Der Veen, and H. L. Ploegh, “A microengraving method for rapid selection of single cells producing antigen-specific antibodies,” *Nat. Biotechnol.*, vol. 24, no. 6, pp. 703–707, 2006.

[38] M. P. Raphael, J. A. Christodoulides, J. B. Delehanty, J. P. Long, and J. M. Byers, “Quantitative imaging of protein secretions from single cells in real time,” *Biophys. J.*, vol. 105, no. 3, pp. 602–608, 2013.

[39] S. Wang *et al.*, “Subcellular resolution mapping of endogenous cytokine secretion by nano-plasmonic-resonator sensor array,” *Nano Lett.*, vol. 11, no. 8, pp. 3431–3434, 2011.

[40] P. Chen, N. T. Huang, M. T. Chung, T. T. Cornell, and K. Kurabayashi, “Label-free cytokine micro- and nano-biosensing towards personalized medicine of systemic inflammatory disorders,” *Adv. Drug Deliv. Rev.*, vol. 95, pp. 90–103,

2015.

[41] Y. Shirasaki *et al.*, “Real-time single-cell imaging of protein secretion,” *Sci. Rep.*, vol. 4, 2014.

[42] A. L. Mattheyses, S. M. Simon, and J. Z. Rappoport, “Imaging with total internal reflection fluorescence microscopy for the cell biologist,” *J. Cell Sci.*, vol. 123, no. 21, pp. 3621–3628, 2010.

[43] M. Huse, B. F. Lillemeier, M. S. Kuhns, D. S. Chen, and M. M. Davis, “T cells use two directionally distinct pathways for cytokine secretion,” *Nat. Immunol.*, vol. 7, no. 3, pp. 247–255, 2006.

[44] A. Gérard *et al.*, “Secondary T cell-T cell synaptic interactions drive the differentiation of protective CD8+ T cells,” *Nat. Immunol.*, vol. 14, no. 4, pp. 356–363, 2013.

[45] Z. L. Zi, J. G. Lock, L. A. Hammond, N. L. La Gruta, J. L. Stow, and P. A. Gleeson, “A trans-Golgi network golgin is required for the regulated secretion of TNF in activated macrophages in vivo,” *Proc. Natl. Acad. Sci. U. S. A.*, vol. 105, no. 9, pp. 3351–3356, 2008.

[46] J. L. Stow, P. Ching Low, C. Offenhäuser, and D. Sangermani, “Cytokine secretion in macrophages and other cells: Pathways and mediators,” *Immunobiology*, vol. 214, no. 7, pp. 601–612, 2009.

[47] X. Tan, J. Heureaux, and A. P. Liu, “Cell spreading area regulates clathrin-coated pit dynamics on micropatterned substrate,” *Integr. Biol. (United Kingdom)*, vol. 7, no. 9, pp. 1033–1043, 2015.

[48] L. K. Rosselli-Murai *et al.*, “Loss of PTEN promotes formation of signaling-capable clathrin-coated pits,” *J. Cell Sci.*, vol. 131, no. 8, 2018.

[49] T. Hyvärinen *et al.*, “Co-stimulation with IL-1β and TNF-α induces an inflammatory reactive astrocyte phenotype with neurosupportive characteristics in a human pluripotent stem cell model system,” *Sci. Rep.*, vol. 9, no. 1, pp. 1–15, 2019.

[50] S. A. Liddelow and B. A. Barres, “Reactive Astrocytes: Production, Function, and Therapeutic Potential,” *Immunity*, vol. 46, no. 6. Elsevier Inc., pp. 957–967, 2017.

[51] R. B. Huang and O. Eniola-Adefeso, “Shear stress modulation of IL-1β-induced E-selectin expression in human endothelial cells,” *PLoS One*, vol. 7, no. 2, pp. 1–9, 2012.

[52] C. W. Tsao, Y. C. Cheng, and J. H. Cheng, “Fluid flow shear stress stimulation on a multiplex microfluidic device for rat bone marrow stromal cell differentiation enhancement,” *Micromachines*, vol. 6, no. 12, pp. 1996–2009, 2015.

[53] E. Michalaki, V. N. Surya, G. G. Fuller, and A. R. Dunn, “Perpendicular alignment of lymphatic endothelial cells in response to spatial gradients in wall shear stress,” *Commun. Biol.*, vol. 3, no. 1, pp. 1–9, 2020.

[54] J. L. Zamanian *et al.*, “Genomic analysis of reactive astrogliosis,” *J. Neurosci.*, vol. 32, no. 18, pp. 6391–6410, 2012.

[55] A. Oyler-Yaniv *et al.*, “A Tunable Diffusion-Consumption Mechanism of Cytokine Propagation Enables Plasticity in Cell-to-Cell Communication in the Immune System,” *Immunity*, vol. 46, no. 4, pp. 609–620, 2017.

[56] J. Bagnall *et al.*, “Quantitative analysis of competitive cytokine signaling predicts tissue thresholds for the propagation of macrophage activation,” *Sci. Signal.*, vol. 11, no. 540, pp. 1–16, 2018.

[57] K. Thurley, D. Gerecht, E. Friedmann, and T. Höfer, “Three-dimensional gradients of cytokine signaling between T cells,” *PLoS Comput. Biol.*, vol. 11, no. 4, pp. 1–22, 2015.

[58] B. D. Winslow, M. B. Christensen, W. K. Yang, F. Solzbacher, and P. A. Tresco, “A comparison of the tissue response to chronically implanted Parylene-C-coated and uncoated planar silicon microelectrode arrays in rat cortex,” *Biomaterials*, vol. 31, no. 35, pp. 9163–9172, 2010.

[59] S. M. Gutowski *et al.*, “Host response to microgel coatings on neural electrodes implanted in the brain,” *J. Biomed. Mater. Res. - Part A*, vol. 102, no. 5, pp. 1486–1499, 2014.

[60] S. Sommakia, J. Gaire, J. L. Rickus, and K. J. Otto, “Resistive and reactive changes to the impedance of intracortical microelectrodes can be mitigated with polyethylene glycol under acute in vitro and in vivo settings,” *Front. Neuroeng.*, vol. 7, no. AUG, pp. 1–8, 2014.

[61] A. Alovskaya, T. Alekseeva, J. B. Phillips, V. King, and R. Brown, “Fibronectin, Collagen, Fibrin-Components of Extracellular Matrix for Nerve regeneration,” *Top. Tissue Eng.*, vol. 3, pp. 1–27, 2007.

[62] J. B. Phillips, V. R. King, Z. Ward, R. A. Porter, J. V Priestley, and R. A. Brown, “Fluid shear in viscous fibronectin gels allows aggregation of fibrous materials for

CNS tissue engineering," *Biomaterials*, vol. 25, no. 14, pp. 2769–2779, 2004.

[63] A. Shinde *et al.*, "Autocrine fibronectin inhibits breast cancer metastasis," *Mol. Cancer Res.*, vol. 16, no. 10, pp. 1579–1589, 2018.

[64] N. D. Gallant, J. R. Capadona, A. B. Frazier, D. M. Collard, and A. J. García, "Micropatterned surfaces to engineer focal adhesions for analysis of cell adhesion strengthening," *Langmuir*, vol. 18, no. 14, pp. 5579–5584, 2002.

[65] L. Karumbaiah *et al.*, "The upregulation of specific interleukin (IL) receptor antagonists and paradoxical enhancement of neuronal apoptosis due to electrode induced strain and brain micromotion," *Biomaterials*, vol. 33, no. 26, pp. 5983–5996, 2012.

[66] C. A. Harris and J. P. McAllister, "What we should know about the cellular and tissue response causing catheter obstruction in the treatment of hydrocephalus," *Neurosurgery*, vol. 70, no. 6, pp. 1589–1601, 2012.

[67] M. E. Ballestas and E. N. Benveniste, "Interleukin 1-β- and tumor necrosis factor-α-mediated regulation of ICAM-1 gene expression in astrocytes requires protein kinase C activity," *Glia*, vol. 14, pp. 267–78, 1995.

[68] S. J. Lee *et al.*, "ICAM-1-Induced Expression of Proinflammatory Cytokines in Astrocytes: Involvement of Extracellular Signal-Regulated Kinase and p38 Mitogen-Activated Protein Kinase Pathways," *J. Immunol.*, vol. 165, no. 8, pp. 4658–4666, 2000.

[69] S. Kyrkanides, J. A. Olschowka, J. P. Williams, J. T. Hansen, and M. K. O'Banion, "TNFα and IL-1β mediate intercellular adhesion molecule-1 induction

via microglia-astrocyte interaction in CNS radiation injury," *J. Neuroimmunol.*, vol. 95, no. 1–2, pp. 95–106, 1999.

[70] S. A. Liddelow *et al.*, "Neurotoxic reactive astrocytes are induced by activated microglia," *Nature*, vol. 541, no. 7638, pp. 481–487, 2017.

[71] M. A. Anderson *et al.*, "Astrocyte scar formation AIDS central nervous system axon regeneration," *Nature*, vol. 532, no. 7598, pp. 195–200, 2016.

[72] I. B. Wanner *et al.*, "Glial scar borders are formed by newly proliferated, elongated astrocytes that interact to corral inflammatory and fibrotic cells via STAT3-dependent mechanisms after spinal cord injury," *J. Neurosci.*, vol. 33, no. 31, pp. 12870–12886, 2013.

[73] S. A. Liddelow, "Modern approaches to investigating non-neuronal aspects of Alzheimer's disease," *FASEB J.*, vol. 33, no. 2, pp. 1528–1535, 2019.

[74] Y. Zhang *et al.*, "Purification and Characterization of Progenitor and Mature Human Astrocytes Reveals Transcriptional and Functional Differences with Mouse," *Neuron*, vol. 89, no. 1, pp. 37–53, 2016.

[75] S. Lutz, C. Raine, and C. Brosnan, "Astrocyte Involvement in the Acquired Demyelinating Diseases," pp. 283–310, 2011.

[76] G. Habiyaremye *et al.*, "Chemokine and cytokine levels in the lumbar cerebrospinal fluid of preterm infants with post-hemorrhagic hydrocephalus," *Fluids Barriers CNS*, vol. 14, no. 1, pp. 1–10, 2017.

[77] G. Ramesh, A. G. Maclean, and M. T. Philipp, "Cytokines and chemokines at the crossroads of neuroinflammation, neurodegeneration, and neuropathic pain,"

Mediators Inflamm., 2013.

[78] J. K. Karimy *et al.*, “Inflammation in acquired hydrocephalus: pathogenic mechanisms and therapeutic targets,” *Nat. Rev. Neurol.*, vol. 16, no. 5, pp. 285–296, 2020.

[79] C. A. Dinarello, A. Simon, and J. W. M. Van Der Meer, “Treating inflammation by blocking interleukin-1 in a broad spectrum of diseases,” *Nat. Rev. Drug Discov.*, vol. 11, no. 8, pp. 633–652, 2012.

[80] J. Xi and H. Liu, “Recent Advances in the Design of Self-Delivery Amphiphilic Drugs and Vaccines,” *Adv. Ther.*, vol. 3, no. 2, p. 1900107, 2020.

[81] R. Biran, D. C. Martin, and P. A. Tresco, “Neuronal cell loss accompanies the brain tissue response to chronically implanted silicon microelectrode arrays,” *Exp. Neurol.*, vol. 195, no. 1, pp. 115–126, 2005.

[82] J. Kestle *et al.*, “Long-term follow-up data from the shunt design trial,” *Pediatr. Neurosurg.*, vol. 33, no. 5, pp. 230–236, 2000.

[83] “Medtronic Inc. Rivulet,” *United States Pat. Ser. No.78887628, 2006*.

[84] M. Galarza *et al.*, “Next generation of ventricular catheters for hydrocephalus based on parametric designs,” *Child’s Nerv. Syst.*, vol. 34, no. 2, pp. 267–276, 2018.

[85] S. Feng, S. Mao, Q. Zhang, W. Li, and J. M. Lin, “Online analysis of drug toxicity to cells with shear stress on an integrated microfluidic chip,” *ACS Sensors*, vol. 4, no. 2, pp. 521–527, 2019.

[86] M. Marimuthu and S. Kim, “Pumpless steady-flow microfluidic chip for cell

culture,” *Anal. Biochem.*, vol. 437, no. 2, pp. 161–163, 2013.

[87] K. W. Selmaj, M. Farooq, W. T. Norton, and C. S. Raine, “Proliferation of astrocytes in vitro in response to cytokines . A primary role for tumor necrosis factor . This information is current as K W Selmaj , M Farooq , W T Norton , C S Raine and C F Why The JI ? Submit online . • Rapid Reviews ! 30 days * from,” 1990.

[88] M. Vinchon, H. Rekate, and A. V. Kulkarni, “Pediatric hydrocephalus outcomes: a review,” *Fluids Barriers CNS*, vol. 9, no. 1, pp. 1–10, 2012.

[89] M. Vinchon, M. Baroncini, and I. Delestret, “Adult outcome of pediatric hydrocephalus,” *Child’s Nerv. Syst.*, vol. 28, no. 6, pp. 847–854, 2012.

[90] J. J. Stone, C. T. Walker, M. Jacobson, V. Phillips, and H. J. Silberstein, “Revision rate of pediatric ventriculoperitoneal shunts after 15 years: Clinical article,” *J. Neurosurg. Pediatr.*, vol. 11, no. 1, pp. 15–19, 2013.

[91] J. M. Drake, J. R. Kestle, and S. Tuli, “CSF shunts 50 years on--past, present, and future.,” *Childs Nerv. Syst.*, vol. 16, no. 10–11, pp. 800–804, 2000.

[92] S. R. Browd, B. T. Ragel, O. N. Gottfried, and J. R. W. Kestle, “Failure of cerebrospinal fluid shunts: Part I: Obstruction and mechanical failure,” *Pediatr. Neurol.*, vol. 34, no. 2, pp. 83–92, 2006.

[93] S. Pujari, S. Kharkar, P. Metellus, J. Shuck, M. A. Williams, and D. Rigamonti, “Normal pressure hydrocephalus: Long-term outcome after shunt surgery,” *J. Neurol. Neurosurg. Psychiatry*, vol. 79, no. 11, pp. 1282–1286, 2008.

[94] B. W. Hanak, E. F. Ross, C. A. Harris, S. R. Browd, and W. Shain, “Toward a

better understanding of the cellular basis for cerebrospinal fluid shunt obstruction: report on the construction of a bank of explanted hydrocephalus devices," *J. Neurosurg. Pediatr.*, vol. 18, no. 2, pp. 213–223, Aug. 2016.

[95] M. R. Del Bigio and J. E. Bruni, "Changes in periventricular vasculature of rabbit brain following induction of hydrocephalus and after shunting," *J. Neurosurg.*, vol. 69, no. 1, pp. 115–120, 1988.

[96] C. A. Harris, D. M. Morales, R. Arshad, J. P. McAllister, and D. D. Limbrick, "Cerebrospinal fluid biomarkers of neuroinflammation in children with hydrocephalus and shunt malfunction," *Fluids Barriers CNS*, vol. 18, no. 1, pp. 1–14, 2021.

[97] K. A. Guttenplan *et al.*, "Knockout of reactive astrocyte activating factors slows disease progression in an ALS mouse model," *Nat. Commun.*, vol. 11, no. 1, pp. 1–9, 2020.

[98] L. E. Clarke, S. A. Liddelow, C. Chakraborty, A. E. Münch, M. Heiman, and B. A. Barres, "Normal aging induces A1-like astrocyte reactivity," *Proc. Natl. Acad. Sci. U. S. A.*, vol. 115, no. 8, pp. E1896–E1905, 2018.

[99] L. C. Foo *et al.*, "Development of a method for the purification and culture of rodent astrocytes," *Neuron*, vol. 71, no. 5, pp. 799–811, 2011.

[100] K. A. Guttenplan *et al.*, "Neurotoxic Reactive Astrocytes Drive Neuronal Death after Retinal Injury," *Cell Rep.*, vol. 31, no. 12, 2020.

[101] D. P. Q. Clark *et al.*, "Inflammation in Traumatic Brain Injury: Roles for Toxic A1 Astrocytes and Microglial–Astrocytic Crosstalk," *Neurochem. Res.*, vol. 44, no. 6,

pp. 1410–1424, 2019.

[102] H. Duan *et al.*, “Transcriptome analyses reveal molecular mechanisms underlying functional recovery after spinal cord injury,” *Proc. Natl. Acad. Sci. U. S. A.*, vol. 112, no. 43, 2015.

[103] Y. Ding *et al.*, “Astrogliosis inhibition attenuates hydrocephalus by increasing cerebrospinal fluid reabsorption through the glymphatic system after germinal matrix hemorrhage,” *Exp. Neurol.*, vol. 320, no. May, p. 113003, 2019.

[104] W. Kang, F. Balordi, N. Su, L. Chen, G. Fishell, and J. M. Hébert, “Astrocyte activation is suppressed in both normal and injured brain by FGF signaling,” *Proc. Natl. Acad. Sci. U. S. A.*, vol. 111, no. 29, 2014.

[105] M. K. Gottipati, A. R. D’Amato, A. M. Ziemba, P. G. Popovich, and R. J. Gilbert, “TGFβ3 is neuroprotective and alleviates the neurotoxic response induced by aligned poly-L-lactic acid fibers on naïve and activated primary astrocytes,” *Acta Biomater.*, vol. 117, pp. 273–282, 2020.

[106] Q. Zhang, H. Gong, W. Gao, and L. Zhang, “Recent progress in capturing and neutralizing inflammatory cytokines,” *CCS Chem.*, vol. 2, no. 3, pp. 376–389, 2020.

[107] L. W. Tien, F. Wu, M. D. Tang-Schomer, E. Yoon, F. G. Omenetto, and D. L. Kaplan, “Silk as a multifunctional biomaterial substrate for reduced glial scarring around brain-penetrating electrodes,” *Adv. Funct. Mater.*, vol. 23, no. 25, pp. 3185–3193, 2013.

[108] T. Fu, Q. Kong, H. Sheng, and L. Gao, “Value of Functionalized

Superparamagnetic Iron Oxide Nanoparticles in the Diagnosis and Treatment of Acute Temporal Lobe Epilepsy on MRI," *Neural Plast.*, 2016.

[109] L. Alvarez-Erviti, Y. Seow, H. Yin, C. Betts, S. Lakhal, and M. J. A. Wood, "Delivery of siRNA to the mouse brain by systemic injection of targeted exosomes," *Nat. Biotechnol.*, vol. 29, no. 4, pp. 341–345, 2011.

[110] X. Luan, K. Sansanaphongpricha, I. Myers, H. Chen, H. Yuan, and D. Sun, "Engineering exosomes as refined biological nanoplatforms for drug delivery," *Acta Pharmacol. Sin.*, vol. 38, no. 6, pp. 754–763, 2017.

[111] S. Cabre, V. Alamilla, N. Moriarty, A. Pandit, and E. Dowd, "Anti-inflammatory cytokine-eluting collagen hydrogel reduces the host immune response to dopaminergic cell transplants in a rat model of Parkinson's disease," *Neuronal Signal.*, 2021.

[112] C. Liu *et al.*, "Surface Modifications of an Organic Polymer-Based Microwire Platform for Sustained Release of an Anti-Inflammatory Drug," *ACS Appl. Bio Mater.*, vol. 3, no. 7, pp. 4613–4625, 2020.

[113] A. P. H. Huang, D. M. Lai, Y. H. Hsu, H. H. Tsai, C. Y. Su, and S. hui Hsu, "An anti-inflammatory gelatin hemostatic agent with biodegradable polyurethane nanoparticles for vulnerable brain tissue," *Mater. Sci. Eng. C*, vol. 121, no. 1, p. 111799, 2021.

[114] D. Zhang *et al.*, "Dealing with the Foreign-Body Response to Implanted Biomaterials: Strategies and Applications of New Materials," *Adv. Funct. Mater.*, vol. 31, no. 6, pp. 1–22, 2021.

[115] R. Whitaker, B. Hernaez-Estrada, R. M. Hernandez, E. Santos-Vizcaino, and K. L. Spiller, “Immunomodulatory Biomaterials for Tissue Repair,” *Chem. Rev.*, vol. 121, no. 18, pp. 11305–11335, 2021.

[116] K. A. Potter-Baker *et al.*, “Development of superoxide dismutase mimetic surfaces to reduce accumulation of reactive oxygen species for neural interfacing applications,” *J. Mater. Chem. B*, vol. 2, no. 16, pp. 2248–2258, 2014.

[117] G. Wei *et al.*, “Polydopamine-Decorated Microcomposites Promote Functional Recovery of an Injured Spinal Cord by Inhibiting Neuroinflammation,” *ACS Appl. Mater. Interfaces*, 2021.

[118] P. T. Hammond, “Layer-by-Layer Approaches to Staging Medicine from Surfaces,” *AIChE J.*, 2015.

[119] Y. He *et al.*, “Synthetic Lift-off Polymer beneath Layer-by-Layer Films for Surface-Mediated Drug Delivery,” *ACS Macro Lett.*, vol. 6, no. 11, pp. 1320–1324, 2017.

[120] J. J. Richardson, M. Björnmalm, and F. Caruso, “Technology-driven layer-by-layer assembly of nanofilms,” *Science (80-.).*, vol. 348, no. 6233, 2015.

ABSTRACT

NEUROPROSTHETIC DEVICE FAILURE ANALYSIS: IMPACT OF SHEAR STRESS AND BLOOD-BRAIN BARRIER DISRUPTION

by

FATEMEH KHODADADEI

May 2022

Advisor: Dr. Carolyn Harris

Major: Materials Science and Engineering

Degree: Doctor of Philosophy

It has been hypothesized that physiological shear forces acting on medical devices implanted in the brain significantly accelerate the rate to device failure in patients with chronically indwelling neuroprosthetics. In hydrocephalus shunt devices, shear forces arise from cerebrospinal fluid (CSF) flow. The shunt's unacceptably high failure rate is mostly due to obstruction with adherent inflammatory cells. Astrocytes are the dominant cell type bound directly to obstructing shunts, rapidly manipulating their activation via shear stress-dependent cytokine secretion. Here we developed a total internal reflection fluorescence microscopy (TIR-FM) combined with a microfluidic shear device chip (MSDC) for quantitative analysis and direct spatial-temporal mapping of secreted cytokines at the single-cell level under physiological shear stress to identify the root cause for shunt failure. Real-time secretion imaging enabled successful detection of a significant increase of astrocyte IL-6 cytokine secretion under shear stress greater than 0.5 dyne/cm^2, validating our hypothesis and highlighting the importance of reducing shear stress activation of cells.

The tissue obstructing neuroprosthetic devices is largely composed of inflammatory cells with a significant astrocyte component. In a first of its kind study, we profile the astrocyte phenotypes present on hydrocephalus shunts. qPCR and RNA in-situ hybridization were used to quantify pro-inflammatory (A1) and anti-inflammatory (A2) reactive astrocytes by analyzing C3 and EMP1 genes, respectively. Additionally, CSF cytokine levels were quantified using ELISA. The results showed a heterogeneous population of A1 and A2 reactive astrocytes on the shunts with obstructed shunts having a significantly higher fraction of A2 astrocytes. The pro-A2 cytokine IL-6 was also found at higher concentrations among CSF from obstructed samples. Furthermore, cytokine neutralizing antibodies produced a significant reduction in both A1 and A2 astrocyte activation and attachment in an in vitro model of astrocyte growth on shunts. Therefore, targeting cytokines involved with astrocyte activation is a promising intervention aimed to prevent shunt obstruction.

AUTOBIOGRAPHICAL STATEMENT

FATEMEH KHODADADEI

Education

- Ph.D. (GPA: 3.95/4.0) 2017-2022

  Chemical Engineering and Materials Science, Wayne State University, MI, US

Publications

- F. Khodadadei, et al. “The effect of A1/A2 reactive astrocyte expression on hydrocephalus shunt failure”, bioRxiv, 2021
- F. Khodadadei, et al. “A high-resolution real-time quantification of astrocyte cytokine secretion under shear stress for investigating hydrocephalus shunt failure”, Communications Biology 4, 2021
- F. Khodadadei, et al. “Methotrexate-loaded nitrogen-doped graphene quantum dots nanocarriers as an efficient anticancer drug delivery system”, Materials Science and Engineering: C 79, p:280-285, 2017
- F. Khodadadei, et al. “Folic acid functionalized vertically aligned carbon nanotube (FA-VACNT) electrodes for cancer sensing applications; suitable for monitoring in time evolution”, Journal of Materials Science & Technology 32, p:617-625, 2016
- F. Khodadadei, et al. “Rapid and clean amine functionalization of carbon nanotubes in a dielectric barrier discharge reactor for biosensor development”, Electrochimica Acta 115, p:378-385, 2014